Resource

Cell

Proteomic Analysis of Unbounded Cellular Compartments: Synaptic Clefts

Graphical Abstract

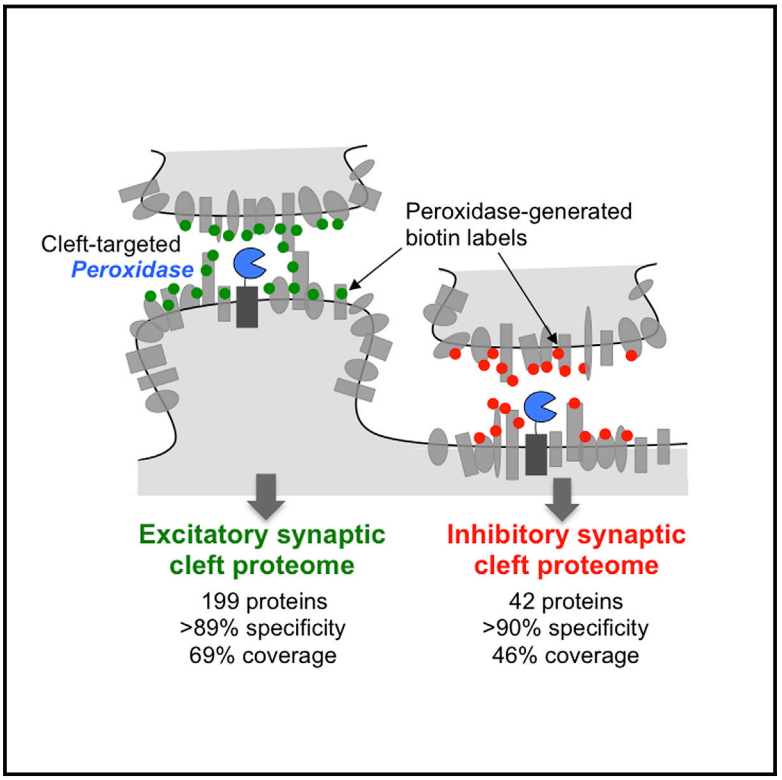

Authors

Ken H. Loh, Philipp S. Stawski, Austin S. Draycott, ..., Beth Stevens, Steven A. Carr, Alice Y. Ting

Correspondence

ayting@stanford.edu

In Brief

An approach enabling proteomic analysis of subcellular compartments that are not membrane enclosed reveals unique features of excitatory and inhibitory synapses.

Highlights

- APEX proteomics extended to open cellular domains, cell surface, and primary cells
- 199 glutamatergic and 42 GABAergic synaptic cleft proteins enriched
- Ten candidates validated as synaptic proteins by imaging and/or synaptosome blotting
- Mdga2 regulates specificity of presynaptic recruitment to inhibitory post-synapses

Loh et al., 2016, Cell *166*, 1295–1307
August 25, 2016
http://dx.doi.org/10.1016/j.cell.2016.07.041

CellPress

Resource

Cell

Proteomic Analysis of Unbounded Cellular Compartments: Synaptic Clefts

Ken H. Loh,[1] Philipp S. Stawski,[1] Austin S. Draycott,[1] Namrata D. Udeshi,[2] Emily K. Lehrman,[3] Daniel K. Wilton,[3] Tanya Svinkina,[2] Thomas J. Deerinck,[4,5] Mark H. Ellisman,[4,5] Beth Stevens,[3] Steven A. Carr,[2] and Alice Y. Ting[1,2,6,7,*]

[1]Department of Chemistry, Massachusetts Institute of Technology (MIT), Cambridge, MA 02139, USA
[2]Broad Institute of MIT and Harvard, Cambridge, MA 02142, USA
[3]F.M. Kirby Neurobiology Center, Boston Children's Hospital (BCH) and Harvard Medical School (HMS), Boston, MA 02115, USA
[4]National Center for Microscopy and Imaging Research, University of California at San Diego, La Jolla, CA 92093 USA
[5]Department of Neurosciences, University of California at San Diego, La Jolla, CA 92093, USA
[6]Present Adress: Stanford University, Departments of Genetics, Biology, and Chemistry, 318 Campus Drive, Stanford, CA 94305-5014, USA
[7]Lead Contact
*Correspondence: ayting@stanford.edu
http://dx.doi.org/10.1016/j.cell.2016.07.041

SUMMARY

Cellular compartments that cannot be biochemically isolated are challenging to characterize. Here we demonstrate the proteomic characterization of the synaptic clefts that exist at both excitatory and inhibitory synapses. Normal brain function relies on the careful balance of these opposing neural connections, and understanding how this balance is achieved relies on knowledge of their protein compositions. Using a spatially restricted enzymatic tagging strategy, we mapped the proteomes of two of the most common excitatory and inhibitory synaptic clefts in living neurons. These proteomes reveal dozens of synaptic candidates and assign numerous known synaptic proteins to a specific cleft type. The molecular differentiation of each cleft allowed us to identify Mdga2 as a potential specificity factor influencing Neuroligin-2′s recruitment of presynaptic neurotransmitters at inhibitory synapses.

INTRODUCTION

The mammalian brain is capable of complex cognition because individual nerve cells assemble into higher order circuits that receive, process, store, and transmit information. Central to this information flow are chemical synapses, specialized junctions between communicating neurons that mediate neurotransmitter release and recognition. Because synapses' functions, along with their formation, remodeling, and elimination, are so central to brain function, there is tremendous interest in dissecting the molecular architecture and functional properties of synapses.

Microscopy and mass spectrometry (MS)-based proteomics have been applied extensively to study the protein composition of synapses. Though powerful in its ability to provide spatial context, microscopy is limited when specific antibodies against target proteins are not available or when recombinant tagging raises concerns about mislocalization or overexpression. Microscopy is also low throughput and more often applied to validate hypotheses than to perform an unbiased search for novel proteins.

MS-based proteomics, on the other hand, is ideally suited for high-throughput and unbiased detection of endogenous proteins. However, it sacrifices spatial information because analysis is performed after cell lysis. Fractionation schemes, such as to enrich entire synaptic terminals (i.e., synaptosomes) (Biesemann et al., 2014), synaptic vesicles (Takamori et al., 2006), the post-synaptic density (PSD) (Bayés et al., 2012), and the active zone (Boyken et al., 2013), recover some spatial information but vary greatly in their degrees of purity. For example, mitochondrial, nuclear, and glial (Henn et al., 1976) contaminants are common in synaptosome and PSD preparations, and key proteins are frequently lost (Figure S1). In addition, fractionation usually blends across many synapse types. Synaptosome purifications, for example, do not distinguish between excitatory glutamate-releasing synapses and inhibitory GABA-releasing synapses, whose molecular compositions are quite different, due to their antagonistic functions. Finally, a major limitation of purification-based MS approaches is that many of the subdomains of the synapse are impossible to purify and therefore inaccessible to MS proteomic analysis. This includes the synaptic cleft and the inhibitory post-synaptic region, which lacks a detergent-insoluble "density," in contrast to the excitatory PSD.

Recently, we (Rhee et al., 2013) and others (Roux et al., 2012) have reported approaches to proteomic mapping that bypass the need for organelle or subdomain purification and instead target "promiscuous" tagging enzymes to the subcellular region of interest (APEX or BioID, respectively). In live cells, addition of a small molecule substrate triggers enzyme-catalyzed biotinylation of its neighboring endogenous proteins (Figures 1A and 1B). Subsequently, biotinylated proteins are enriched with streptavidin beads and identified by MS. The main advantages of this approach are that unpurifiable cellular regions, such as the synaptic cleft, can in principle be targeted for proteomic mapping, and the resulting data are potentially more accurate, because tagging is performed in living cells while membranes and protein complexes are still intact and artifacts resulting from detergent lysis and serial centrifugation are avoided.

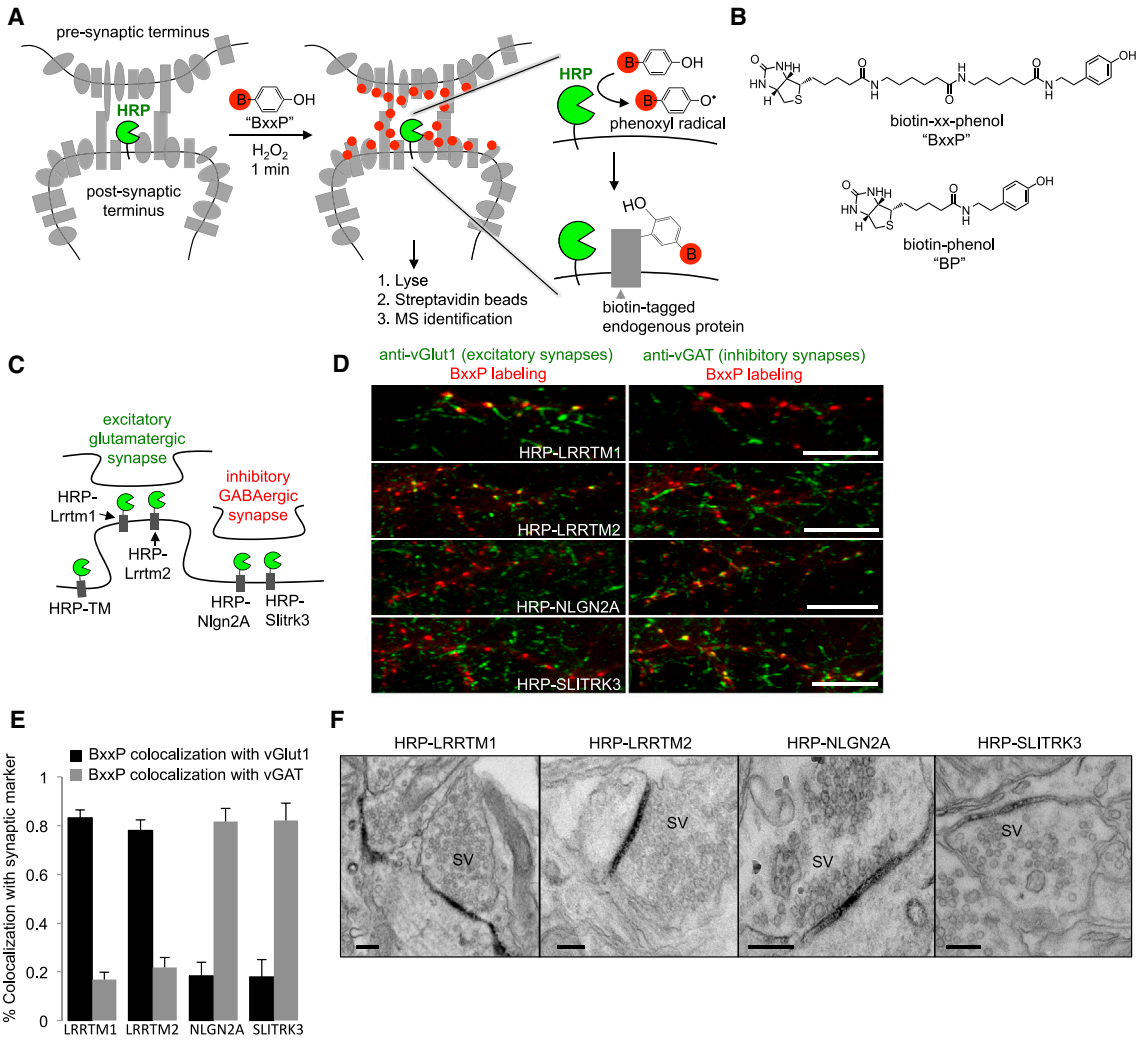

Figure 1. Design and Characterization of Peroxidase Fusion Constructs for Proximity Biotinylation

(A) Scheme of peroxidase-mediated proteomic tagging in the synaptic cleft. Horseradish peroxidase (HRP) is genetically targeted to the cleft via fusion to a known cleft protein. The gray shapes are endogenous proteins residing inside and outside the synapse. To initiate labeling, the membrane impermeant biotin-phenol conjugate BxxP (red B, biotin; chemical structure in B) is added to the live neurons for 1 min together with the oxidant H_2O_2. HRP converts BxxP into a phenoxyl radical, which covalently tags proximal endogenous proteins at electron-rich side chains such as Tyr (Rhee et al., 2013). Subsequently, neurons are lysed and biotinylated proteins are isolated using streptavidin beads for identification by mass spectrometry (MS).

(B) Structure of BxxP and BP probes.

(C) HRP fusion constructs employed in this study. HRP-TM is a general cell-surface construct.

(D) Fluorescence imaging of synaptic HRP fusion constructs with respect to excitatory and inhibitory synapse markers, vGlut1 and vGAT. For maximum detection sensitivity, the HRP constructs were visualized via BxxP labeling followed by neutravidin-AlexaFluor647 staining (red). Scale bars, 10 μm. See also Figures S1–S4 for additional characterization of constructs and their expression levels.

(E) Quantitation of colocalization extent for images in (D) plus seven other fields of view containing >900 puncta per construct. Errors, ± 1 SD

(F) Electron microscopy (EM) of HRP fusion constructs. HRP catalyzes the polymerization and local deposition of diaminobenzidine, which recruits electron-dense osmium (Martell et al., 2012). SV, synaptic vesicles. Scale bars, 200 nm. See also Figure S2C for additional EM.

Though such technology could be highly enabling for the study of synapse molecular architecture, numerous hurdles must be surmounted. First, neither APEX nor BioID have been demonstrated in neurons. Second, we have only used APEX for proteomic mapping in membrane-enclosed compartments (the mitochondrial matrix [Rhee et al., 2013] and mitochondrial intermembrane space [Hung et al., 2014]), not "open" subcellular regions such as the synaptic cleft. It is unclear what spatial specificity is achievable in such an environment. BioID is expected to have a larger labeling radius than APEX, because the half-life of its reactive intermediate, biotin-AMP, is minutes in water, in contrast to <1 ms for the biotin-phenoxyl radical generated by APEX-catalyzed oxidation. Third, synapses constitute a tiny fraction of neurons by mass. It is unclear if existing protocols can enrich a small biotinylated proteome over the much larger non-biotinylated proteome: previous APEX studies have

targeted much more abundant structures, such as mitochondria. Fourth, it is challenging to localize APEX activity specifically to synaptic subdomains of interest. Though cleft-resident proteins are known, all of these also have pools elsewhere in the neuron, such as the secretory pathway. How can we achieve specific proteomic tagging only in the cleft and avoid capturing the endoplasmic reticulum (ER) or Golgi proteomes as well?

Here, we describe modifications to the APEX technique to enable successful proteomic mapping of the neuronal synaptic cleft. To begin to probe the vast diversity of synapses in the brain, we generate two independent proteomic lists: one representative of excitatory, glutamate-releasing synapses and one representative of inhibitory, GABA-releasing synapses. We analyze these proteomes to show that specificity and depth of coverage are both higher than for previous proteomes obtained by biochemical fractionation. Follow-up imaging and western blotting provide synapse validation for ten proteomic hits. Finally, we perform functional studies in neuron culture on two post-synaptic membrane proteins identified in our proteomes, Mdga1 and Mdga2, and uncover differences in their regulatory effects on Nlgn2, suggesting potential roles in setting synapse specificity.

RESULTS

Establishing a Peroxidase-Based Platform for Proteomic Mapping of the Synaptic Cleft

Though APEX tagging has been performed in *Drosophila* larval muscle (Chen et al., 2015), reagent delivery to tissue was a concern, in addition to H_2O_2 toxicity. We therefore opted to use dissociated neuron culture, rather than intact brain tissue, to allow for rapid delivery and washout of biotin-phenol, H_2O_2, and subsequent peroxidase quenchers. At DIV19 (19 days in vitro), our embryonic rat cortical neuron cultures displayed abundant staining of synapse markers (Bassoon, vGlut1, and vGAT), and synapses looked normal by electron microscopy (EM) (Figures 1F and S2C).

When designing the peroxidase fusion constructs to use for proteomic mapping in the synaptic cleft, our first concern was to maximize the activity of the peroxidase, because the proteomic region of interest is so small. APEX2 is the second-generation, more active variant of APEX (Lam et al., 2015). However, the commonly used horseradish peroxidase (HRP) enzyme is even more active than APEX2. For applications in the cytosol, nucleus, and mitochondria, HRP cannot be used, because its four structurally essential disulfide bonds do not form in reducing environments, leaving HRP inactive (Martell et al., 2012). However, HRP is active in the oxidizing secretory pathway and cell surface and catalyzes the same labeling chemistry as APEX2 with biotin-phenol (Rees et al., 2015; Rhee et al., 2013). We therefore generated N-terminal, extracellular-facing fusions of HRP with three known glutamatergic excitatory synaptic cleft-resident proteins (Nlgn1, Lrrtm1, and Lrrtm2 [Linhoff et al., 2009; Song et al., 1999]) and two known GABAergic inhibitory synaptic cleft resident proteins (Slitrk3 and Nlgn2 [Chih et al., 2006; Takahashi et al., 2012; Varoqueaux et al., 2004]) (Figure 1C). Surprisingly, HRP-Nlgn1 exhibited poor specificity for excitatory over inhibitory synapses, by imaging and in a preliminary MS proteomic experiment (Figure S1), and was not characterized further. The remaining four constructs were highly enriched at synapses (Figures S2A and S2B), gave the expected preference for excitatory versus inhibitory synapses (Figure 1D and 1E), and showed specific and robust HRP activity in the cleft by EM (Figures 1F and S2C). Using lentiviral transduction, we titrated down expression levels to 40%–70% that of the endogenous protein or mRNA counterpart (Figures S3A–S3C). Under these expression conditions, we did not observe changes in synapse size or density in transduced neurons (Figures S3E and S3F).

As expected, treatment with biotin-phenol (BP) and H_2O_2 gave labeling of both cell-surface and intracellular proteins, likely in the secretory pathway proximal to ER and Golgi pools of the HRP fused proteins. We reasoned that we could improve specificity for the extracellular cleft proteome by rendering BP membrane impermeant. We synthesized a variant, called BxxP, with a long and polar polyamide linker (Figure 1B). Figure 2A shows that BxxP still gives robust biotinylation with HRP and H_2O_2 but no longer enters cells (no signal observed with intracellular constructs PSD95-APEX2 and APEX2-NES). When applied to the synaptic HRP fusion constructs, BxxP produced HRP- and H_2O_2-dependent biotinylation on the neuron surface that was punctate in appearance (Figures 1D, S4A, and S4B). By contrast, HRP-TM, a control construct that expresses over the entire neuron surface, produced a diffuse rather than punctate BxxP labeling pattern.

We ran biotinylated neuron lysates on gel and analyzed them by streptavidin blotting. Figures S4C and S4D show that each HRP fusion construct biotinylates a wide range of endogenous proteins, in an H_2O_2-dependent manner. However, when we proceeded to enrich these biotinylated proteins using streptavidin-coated beads according to our previous protocol, we found that endogenous cytosolic proteins such as PSD95, which should not be tagged by HRP and BxxP, were also enriched (Figures 2C and 2D). We hypothesized that our previous enrichment protocol was not disassembling the detergent-insoluble and tightly crosslinked post-synaptic density (PSD), which was coming down with the biotinylated cleft proteome. We therefore modified the protocol by adding a 1% SDS lysis step with 10 min boiling to disrupt the PSD and found that this removed undesired cytosolic proteins while preserving enrichment of desired synaptic surface proteins such as GluA1 (Figure 2D). Figure 2B shows streptavidin blot and silver stain visualization of our enriched biotinylated proteomes.

Proteomic Mapping of Excitatory Glutamatergic and Inhibitory GABAergic Synaptic Clefts

Previously, we found that a "ratiometric" APEX-tagging strategy improved the specificity of protein identifications in the mitochondrial intermembrane space (IMS), a compartment that is leaky to biotin phenoxyl radicals, due to porins in the outer mitochondrial membrane (Hung et al., 2016). In the ratiometric approach, for each detected protein, we compare its extent of biotinylation by targeted peroxidase (e.g., synaptic HRP fusion construct) versus non-targeted peroxidase (e.g., HRP-TM, which targets HRP evenly over the entire neuron surface). If a protein is biotinylated more extensively by synaptic HRP than by HRP-TM, we retain it for our proteome. If it is biotinylated

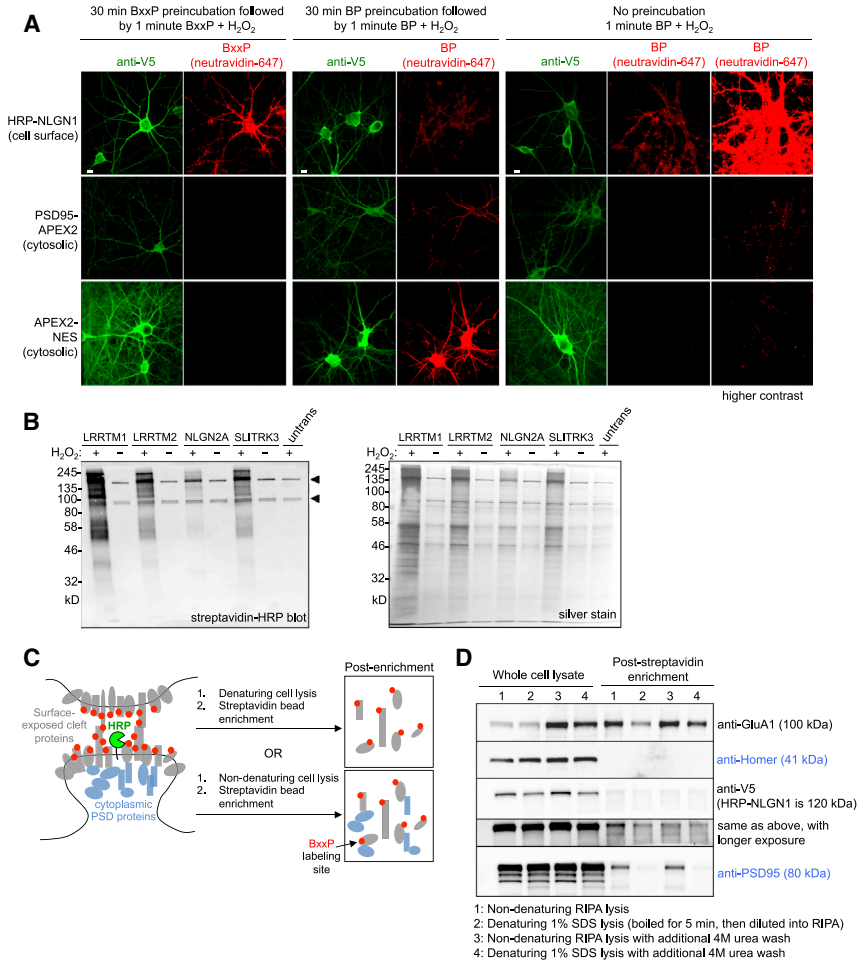

Figure 2. Development of BxxP Probe for Cell-Surface Labeling and Alternative Streptavidin Enrichment Protocol

(A) BxxP is membrane impermeant. Neurons expressing the indicated peroxidase fusion construct (left) were labeled live with BxxP or BP, then fixed and stained. HRP at the cell surface gives biotinylation with both BxxP and BP, whereas intracellular peroxidase fusion constructs show biotinylation with BP only.

(B) Gel analysis of streptavidin-enriched lysates after live-neuron biotinylation with HRP fusion constructs. Untrans, untransfected neurons. Arrowheads point to endogenously biotinylated proteins (Chapman-Smith and Cronan, 1999).

(C) Development of lysis conditions to separate biotinylated cleft proteins from cytosolic post-synaptic density (PSD) proteins. Our standard RIPA lysis (bottom) retrieved many intracellular PSD proteins (blue) along with biotinylated (red) cleft-exposed proteins (gray).

(D) Four different lysis/wash conditions were tested to solubilize the PSD and retrieve proteins biotinylated by HRP-NLGN1 and BxxP. Blotting of streptavidin-enriched lysates for a cleft marker (GluA1) and intracellular markers (Homer and PSD95) showed that conditions 2 and 4 removed the latter while retaining the former. Condition 2 was used for large-scale proteomics. Condition 1 was used in previous studies (Hung et al., 2014; Rhee et al., 2013). The anti-V5 blot detects HRP-NLGN1. See also Figure S4.

more extensively by HRP-TM than by synaptic HRP, we reject it: such proteins may be just outside of synapses, accessible to the biotin radical, but not actually a synaptic protein.

Because the synaptic cleft is open and non-membrane-enclosed, it represents a greater challenge than the mitochondrial IMS in terms of spatial specificity. We reasoned that it would be essential to use the ratiometric tagging approach. We also wanted to capitalize on the availability of two validated HRP fusion constructs for each synaptic cleft type—Lrrtm1 and Lrrtm2 for the excitatory glutamatergic cleft and Slitrk3 and Nlgn2 for the inhibitory GABAergic cleft. An endogenous protein enriched by two different excitatory HRP constructs is much more likely to be a true positive identification than a protein enriched by only one. With these considerations in mind, we designed the three independent proteomic experiments shown in Figure 3A. Each experiment combines four cellular samples: one biotinylated by an excitatory HRP fusion construct; one biotinylated by an inhibitory HRP fusion construct; one biotinylated by HRP-TM; and one non-biotinylated negative control. The four samples are separately lysed and enriched with streptavidin beads. After on-bead trypsin digestion to peptides, chemical iTRAQ tagging is performed to differentiate the samples by mass signature. The four samples are then combined and analyzed as a pooled mixture by liquid chromatography and tandem MS/MS.

As shown in Figure 3B, each experiment identified >2400 unique proteins. The vast majority of these were non-specific streptavidin bead binders, identifiable by their low 114/117 or 115/117 iTRAQ ratios. After removing these proteins ("Filter 1", Figure 3C), we used the 114/116 and 115/116 iTRAQ ratios to identify proteins preferentially enriched by synaptic HRP constructs over the HRP-TM control construct ("Filter 2", Figure 3D). Then, the three independent excitatory synaptic cleft datasets were intersected, as well as the three independent inhibitory synaptic cleft datasets. Figures S5B and S5C illustrate the importance of the three-way intersection to improve the quality of each proteomic list. The last filter ("Filter 3", Figure 3E) was based on excitatory/inhibitory biotinylation ratio: we removed from the excitatory proteome the small number of proteins that were much more strongly biotinylated by inhibitory HRP constructs than excitatory HRP constructs, and vice versa. After these filtering steps, our final excitatory and inhibitory proteomic lists consisted of 199 (Table S1, Tab 1) and 42 (Table S1, Tab 2) unique proteins, respectively.

Characteristics of the Two Proteomic Lists

As expected, each proteomic list contains numerous ion channels, GPCRs, adhesion proteins, and transporters (Figure 4A).

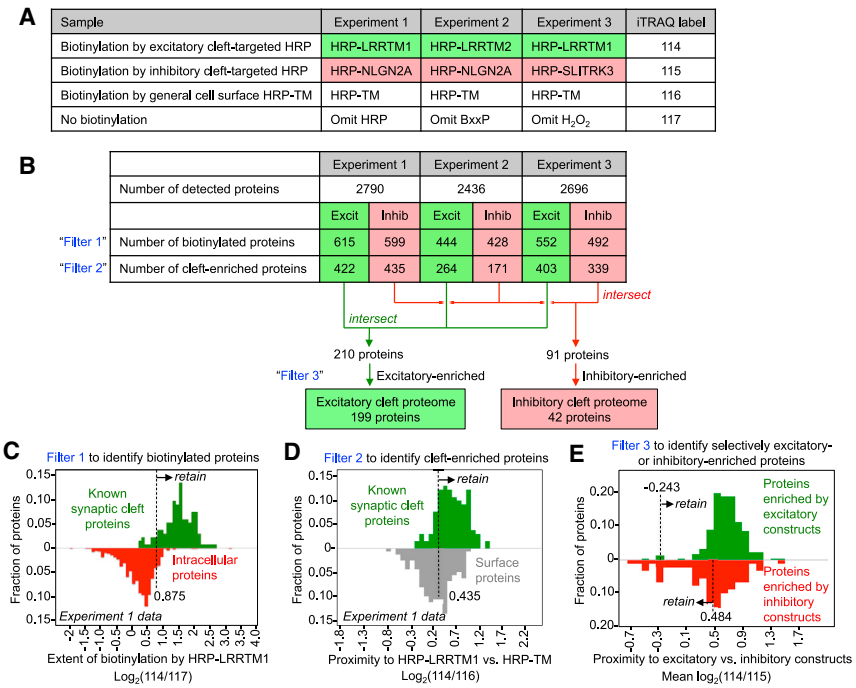

Figure 3. Design of Proteomic Study and Cut-Off Analysis

(A) Design of three independent proteomic experiments. Each experiment consisted of four samples, which were separately enriched and tagged with unique iTRAQ labels (right). Mass spectrometry (MS) was performed on the mixture of four samples, resulting in four mass-shifted peaks of varying intensity per detected peptide.

(B) Filtering of MS data to produce excitatory and inhibitory proteomic lists. The table shows the number of proteins remaining after each filtering step. In the first row, a protein was considered detected if ≥2 unique peptides were sequenced by MS. Filter 1 retains HRP-biotinylated proteins and removes non-specific bead binders, on the basis of 114/117 or 115/117 iTRAQ ratio. Filter 2 retains cleft-enriched proteins over general cell-surface proteins, on the basis of 114/116 or 115/116 iTRAQ ratio. Filter 3 removes strongly inhibitory-enriched proteins (high 115/114 iTRAQ ratio) from the excitatory proteome, and vice versa for the inhibitory proteome.

(C–E) Histograms that illustrate how Filters 1, 2, and 3 were applied. In (C) and (D), green shows the distribution of true positives. Red in (C) is the distribution of false positives. See also Figure S5 and Table S4.

Both post-synaptic membrane proteins and pre-synaptic membrane proteins are represented, in addition to soluble secreted proteins such as Nptx1 (Figure 4B). We also observe some secreted proteins that may be of glial origin, such as Gpc6, which promotes excitatory synapse formation (Allen et al., 2012). Our excitatory synaptic cleft list contains all four AMPA receptor subunits and three NMDA receptor subunits, while seven $GABA_A$ receptor subunits appear in the inhibitory synaptic cleft list. The overlap between the two proteomic lists is 20 proteins (Table S1, Tab 3), which includes known dual-localized synaptic proteins such as Erbb4 (Krivosheya et al., 2008), Grik2 (Lerma, 2003), and Gabbr1 (Kulik et al., 2002).

To characterize the specificity of each proteomic list, we first checked for intracellular cytosolic proteins. Both lists lack any protein known to be intracellular (Table S1, Tabs 1 and 2, Column AN), attesting to the effectiveness of BxxP in restricting biotinylation to the cell surface. We then determined synapse specificity by calculating the fraction of each proteome with prior literature connection to synapses. 84% of the excitatory proteome and 90% of the inhibitory proteome have previous synapse annotation (Figure 4B, left). The remaining 33 proteins (29 from the excitatory proteome, 2 from the inhibitory proteome, and 2 in both; Table S2) that lack synapse annotation, which we call "synapse orphans," could be false positives, or they could be newly discovered synaptic proteins. Below, we present imaging and western blotting data on ten of these synapse orphans, supporting the latter possibility.

To determine the excitatory versus inhibitory synapse specificity of each proteomic list, we analyzed the subset of proteins in each list with known excitatory or inhibitory synapse localization (Figure 4B, middle). The excitatory proteome is highly enriched for proteins known to reside at excitatory synapses or at both synapse types (98%). The inhibitory proteome is enriched for known inhibitory synapse proteins (62%), but also includes a significant number of proteins with excitatory annotation. Because the inhibitory synapse is poorly characterized and the literature is biased toward assays of excitatory synapse localization, it is possible that many of these proteins are actually dual localized to both excitatory and inhibitory synapses. Indeed, follow-up experiments described below and shown in Figure S6 suggest dual localization for four excitatory-annotated proteins that appear in our inhibitory synaptic cleft proteome.

Figure 4C provides an illustration of the synapse subtype specificity of both proteomic lists, showing for example that AMPA and NMDA receptor subunits are detected only in the excitatory proteome, while $GABA_A$ receptor components are detected exclusively in the inhibitory proteome. Interestingly, previous studies have suggested that some inhibitory synapse components "leak over" to excitatory synapses, and vice versa, perhaps to enable cross-talk or regulation between synapse types (Chen et al., 2012). Consistent with these studies, our data show that the inhibitory $GABA_B$ receptor subunit Gabbr1 resides at excitatory synapses as well (Kulik et al., 2002) and the excitatory kainate receptor Grik2 can also be found at inhibitory synapses (Lerma, 2003).

Due to our experimental design, every protein appearing in our lists is associated with an E/I (excitatory/inhibitory) ratio, based on the 114/115 iTRAQ ratio, that reflects its enrichment at excitatory versus inhibitory synapses. This can be visualized in the scatterplots shown in Figures 4D and S5D. Known excitatory synapse-specific proteins such as AMPA receptors (Gria2-3) and NMDA receptors (Grin1) appear below the

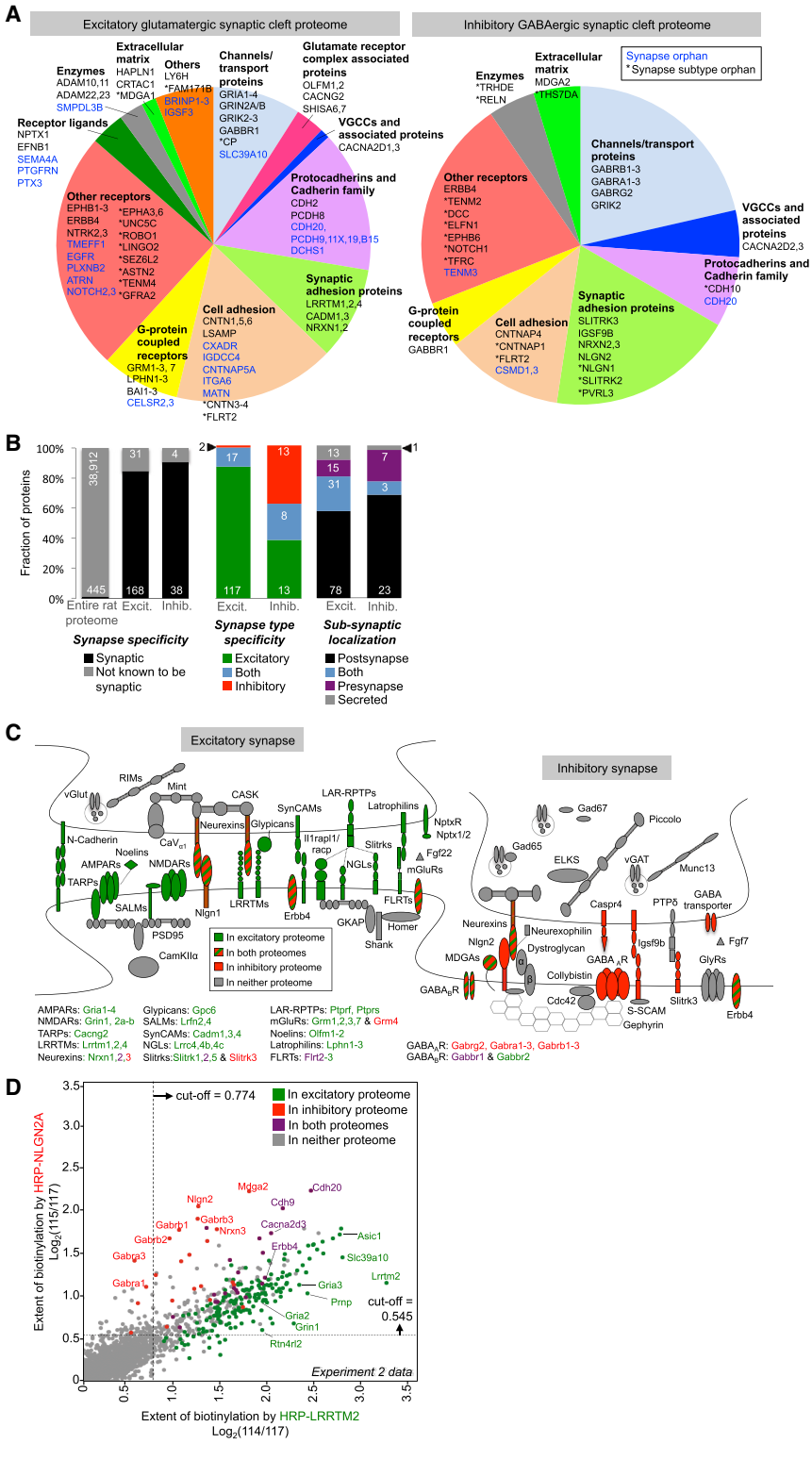

Figure 4. Specificity and Coverage of Excitatory and Inhibitory Synaptic Cleft Proteomes

(A) Proteins of each proteomic list, subdivided by functional class. Genes in blue have no prior connection to synapses (i.e., they are synapse orphans), while genes with asterisks (*) have no prior connection to that specific synapse type (but are known to be generally synaptic).

(B) Graphs showing the synapse specificity (left) and synapse subtype specificity (middle) of the two proteomic lists. Excit., refers to the excitatory proteome of 199 proteins; Inhib., refers to the inhibitory cleft proteome of 42 proteins. For synapse subtype analysis, only proteins with literature annotation as excitatory/inhibitory/both are included in the analysis: non-annotated synaptic proteins are excluded. On the far right, proteins are classified according to their sub-synaptic localization. Further details provided in Table S1, Tabs 1 and 2.

(C) Cartoon depicting well-established excitatory (left) and inhibitory (right) synapse proteins. Proteins are colored according to whether they were detected in our excitatory proteome (green), inhibitory proteome (red), both (striped), or neither (gray). Proteins with multiple isoforms are listed below. Purple font indicates detection in both proteomes.

(D) Scatterplot showing the separation of proteins by E/I (excitatory/inhibitory) ratio. All proteins detected in experiment 2 are plotted, by biotinylation extent in the inhibitory cleft (y axis) versus excitatory cleft (x axis). Each protein is colored according to whether it is present in either final proteomic list. Points corresponding to some well-established inhibitory, excitatory, and dual-localized synaptic proteins are labeled. Dashed lines indicate the cut-offs applied to the data (Filter 1). See also Figure S5D for additional E/I scatterplots.

diagonal, whereas known inhibitory synapse-specific proteins such as $GABA_A$ receptors (Gabra1,3, Gabrb1-3) lie above the diagonal. Dual-localized proteins such as Erbb4 are close to the diagonal.

To characterize the sensitivity, or depth of coverage, of each proteome, we generated separate lists of well-established excitatory cleft-resident or inhibitory cleft-resident proteins (Table S3). Of the 62 such excitatory proteins, our proteome contained 43 (69%). Of the 24 inhibitory proteins, we enriched 11 (46%). The proteins we missed may be sterically shielded from biotinylation through protein or membrane interactions in the live-cell context. Alternatively, they could be dual localized, with both a synaptic population and a non-synaptic population, and consequently removed by our Filter 2 step (Figures 3B and 3D), which considers the ratio of biotinylation by synapse-localized HRP versus general cell-surface HRP-TM. Finally, some genes may not be expressed in the specific rat cortical neuron preparations that we used.

A

Synapse orphans	Evidence for synaptic localization		
	Imaging with Bassoon	Imaging with vGlut1	Immunoblot of synaptosomes
LINGO2	Figure 5B	Figure 5D	
EGF receptor	Figure 5B	Figure 5D	Figure 5E
CXADR	Figure 5B	Figure 5D	
Protocadherin-9 (PCDH9)	Figure 5B	Figure 5D	
BRINP3			Figure 5E
Semaphorin-4A (SEMA4A)			Figure 5E
NOTCH2	Figures 5G,H		Figure 5E
Trophoblast glycoprotein (TPBG)			Figure 5E
Zinc transporter ZIP10 (SLC39A10)			Figure 5E
Integrin alpha-6 (ITGA6)			Figure 5E

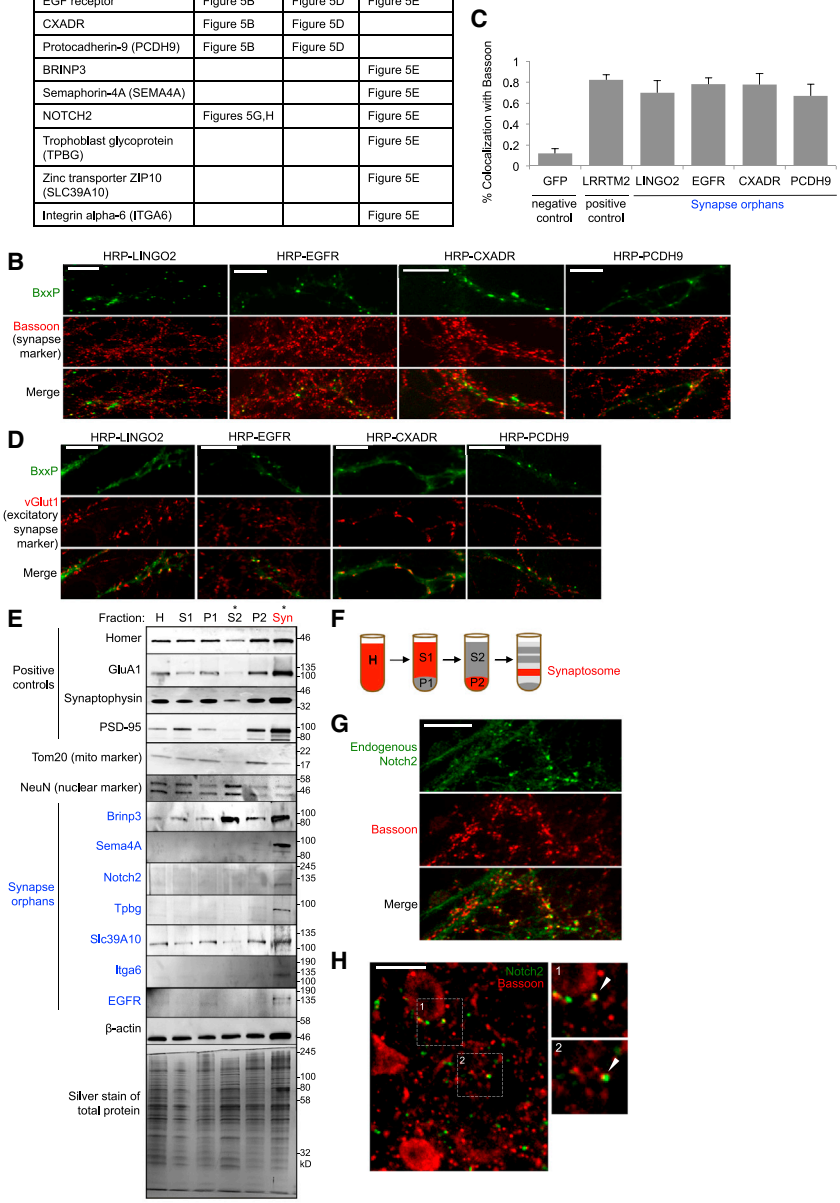

Figure 5. Imaging and Synaptosome Blotting of Specific Proteomic Hits

(A) Table summarizing results. Ten synapse orphans (proteins without prior literature connection to synapses) from our excitatory synaptic cleft proteome were analyzed. Figure panels showing relevant data are given.

(B) Colocalization of four synapse orphans with pre-synaptic marker Bassoon. Genes were fused at their N-terminal ends to HRP and visualized by BxxP labeling followed by neutravidin-Alexa-Fluor647 staining.

(C) Quantitation of data in (B). >8 fields of view were analyzed for each construct. HRP-LRRTM2 was a positive control analyzed in parallel, and GFP was a non-synapse localized negative control. Errors, ± 1 SEM.

(D) Colocalization of orphans in (B) with excitatory synapse marker vGlut1.

(E and F) Immunoblot detection of seven synapse orphans (blue) in purified synaptosomes (Syn) derived from adult rat brain. Tom20 and NeuN are negative controls. Fractions defined in (F). Red tracks the synaptosomes after each fractionation step.

(G and H) Confocal imaging of endogenous Notch2 in DIV19 cultured neurons (G) and adult rat brain tissue (H) along with synapse marker Bassoon. All scale bars, 10 μm. See also Figure S6.

Proteomes Reveal New Synaptic Proteins

Within each proteome, ~85% of proteins have prior literature connection to synapses. The remaining ~15% are "synapse orphans," with no previous literature assigning them to synapses. We found 29 such orphans in the excitatory cleft, 2 in the inhibitory cleft, and 2 in both clefts (some examples in blue font in Figure 4A; complete list of orphans in Table S2, Tab 1). Guided by the availability of commercial antibodies and transgenes for recombinant expression, we selected 14 excitatory synapse orphans for follow-up analysis (Figure 5A).

To perform fluorescence imaging, we expressed 7 recombinant orphan proteins in DIV19 neuron cultures, via lentiviral transduction. We found that extremely low expression levels were essential to observe punctate rather than diffuse localization patterns, perhaps because mistargeting occurs upon overexpression. However, GFP and V5 epitope tags were not visible at such low expression levels; instead, we used HRP in combination with BxxP as a highly sensitive, amplifying imaging label (Figure S6 shows the superior sensitivity of HRP over Venus for fluorescence imaging). Figures 5B and 5D show that four orphan proteins from the excitatory proteome, tagged with HRP at their N-terminal ends, colocalize with endogenous Bassoon as well as vGlut1, a marker of glutamatergic synapses.

For eight synapse orphans, we obtained commercial antibodies and used these to probe for the endogenous proteins in purified synaptosomes derived from adult rat brain. A concern when using neuron cultures is that synapses could form between neurons that do not normally contact each other in vivo. By contrast, our synaptosomes are derived from physiological synapses already present in the adult rat brain. For seven orphans, we observed clear enrichment of the endogenous protein in synaptosome fractions compared to non-synaptosome

fractions such as S2 (Figures 5E and 5F). The eighth antibody, against Notch3, failed to detect Notch3, even in whole neuron lysate (data not shown). Thus, for seven synapse orphans, the combination of enrichment at synaptic clefts in live neuron culture (via HRP tagging) *and* enrichment in synaptosomes derived from adult brain tissue provides strong and orthogonal evidence that these proteins are bona fide synaptic proteins.

One of these antibodies, against Notch2, also worked for visualization of the endogenous protein, both in neuron culture and in adult rat brain tissue. Figures 5G and 5H show colocalization of Notch2 and the synapse marker Bassoon, providing a third line of evidence that Notch2 is synaptically localized.

Altogether, of the 14 synapse orphans we analyzed by imaging and immunoblotting, positive identifications were made for 10 of them (Figure 5A). For the remaining four, two were inconclusive (non-specific antibody for Notch3 and HRP tag disruption of surface trafficking for Matn2). Negative results were obtained for HRP-tagged Brinp2 and Smpdl3b, but we suspect that these soluble, secreted proteins may be especially sensitive to HRP tagging and could mislocalize. This is supported by the observation that HRP-tagged Brinp3 (homologous to Brinp2) also appeared non-synaptic by imaging, but due to availability of a specific antibody for this protein, we were able to assign endogenous Brinp3 to synapses via synaptosome immunoblotting (Figure 5E). Therefore, our statistics, albeit on a small sample size, suggest that our synaptic cleft proteomic lists have very low false-positive rates (i.e., the 84%–90% synapse specificity represents a lower bound) and may be a rich source of synapse protein candidates.

The proteomic datasets can also be mined for insights on the synapse sub-type specificity of known synaptic proteins. For example, for the 38 known synaptic proteins in our inhibitory synaptic cleft list, 17 were not previously known to reside at inhibitory GABAergic synapses specifically. Interestingly, the proteomic lists also highlight 11 proteins previously annotated as excitatory, which we detected at *both* excitatory and inhibitory synapses in our proteomic datasets. To follow up on four of these proteins, we performed fluorescence microscopy with HRP-tagged recombinant proteins introduced by lentiviral transduction. Figure S6 shows that all four of these proteins (Flrt2, EphB6, Dcc, and Elfn1) significantly colocalize with *both* vGlut1 and vGAT markers, suggesting that they reside at both synapse types, at least in neuron culture.

CD200 Is an Excitatory Synapse-Localized Protein that Regulates Synapse Numbers in the Visual Thalamus

For many of the proteins we enriched, the only prior evidence for synaptic localization was enrichment in a synaptosome MS study. As described above, the high false-positive rates of such studies necessitate extensive follow-up experimentation to distinguish true positives from false positives. By contrast, our lists are much more specific. Therefore, if a protein is detected in a synaptosome preparation *and* in our live-cell proteomic map, it is much more likely to be a genuine synaptic protein. CD200 is one of the most highly enriched proteins in our excitatory synaptic cleft proteome. CD200 was previously identified in a synaptosome MS study (Biesemann et al., 2014) (which is why we did not classify it as a synapse orphan), but there has been no further characterization of this protein in neurons. We performed immunostaining of CD200 in brain tissue from wild-type mice and found that it was localized throughout the neuropil, as expected for an excitatory synaptic protein (Figure S6F). In the visual thalamus, CD200 expression was highest during early postnatal development (P10), which could indicate a role in synapse development or remodeling. We then used structured illumination microscopy (SIM) to assess whether CD200 colocalized with synaptic markers in vivo. Indeed, CD200 colocalized with both presynaptic marker vGlut2 and postsynaptic marker Homer in the P10 dorsal lateral geniculate nucleus of the thalamus (dLGN) (Figure S6G).

To probe the functional role of CD200 at synapses, we used high-resolution confocal microscopy to quantify the number of colocalized vGlut2 and Homer puncta in the dLGN of CD200 knockout (KO) mice at P10 (Figures S6H and S6I). We observed a significant reduction in synapse numbers compared to wild-type littermate controls, demonstrating that the function of CD200 is indeed relevant to the synapse. Future studies will be needed to determine whether CD200 plays a role in synapse formation or regulates an aspect of the synaptic refinement process.

Mdga1 and Mdga2 Have Distinct Localizations and Regulatory Functions

The availability of distinct proteomic datasets for the excitatory glutamatergic and inhibitory GABAergic synapses provides an opportunity to consider the complement of molecules that define and contribute to the specific formation of each synapse type. For example, specific synaptic adhesion proteins are known to play important roles in recruiting GABA vesicle-containing pre-synapses to GABA receptor-containing post-synaptic membranes and glutamate vesicle-containing pre-synapses to glutamate receptor-containing post-synaptic membranes.

Our attention was drawn to two proteins, Mdga1 and Mdga2, that have been linked in previous studies to the well-studied adhesion protein Nlgn2. Lee et al. (2013) and Pettem et al. (2013) have shown that both Mdgas bind to Nlgn2 and that Mdga1 acts via Nlgn2 to downregulate inhibitory synapse formation. Due to high (~70%) sequence homology, Mdga2 was assumed to have the same localization and function as Mdga1, though Mdga2 has not previously been studied in neurons. Interestingly, we detected Mdga1 in our excitatory synaptic cleft proteome and Mdga2 in our inhibitory proteome, which challenges this assumption and suggests that Mdga2 may have a different function at synapses than Mdga1.

To further investigate Mdga1 and Mdga2, we prepared recombinant fusions to HRP, since specific antibodies are not available, and imaged the proteins in DIV19 neurons. In agreement with the proteomic data, recombinant Mdga2 overlapped with the inhibitory marker vGAT exclusively (Figure 6A). Recombinant Mdga1, on the other hand, overlapped with both excitatory and inhibitory markers (Figure S7A). The discrepancy between this observation and our proteomic data could result from the incomplete coverage of the inhibitory proteome, which recalled only 46% of expected proteins. Previous imaging of GFP-Mdga1 also showed overlap with both excitatory and inhibitory terminals (Pettem et al., 2013). Thus, Mdga1 is most likely localized to both

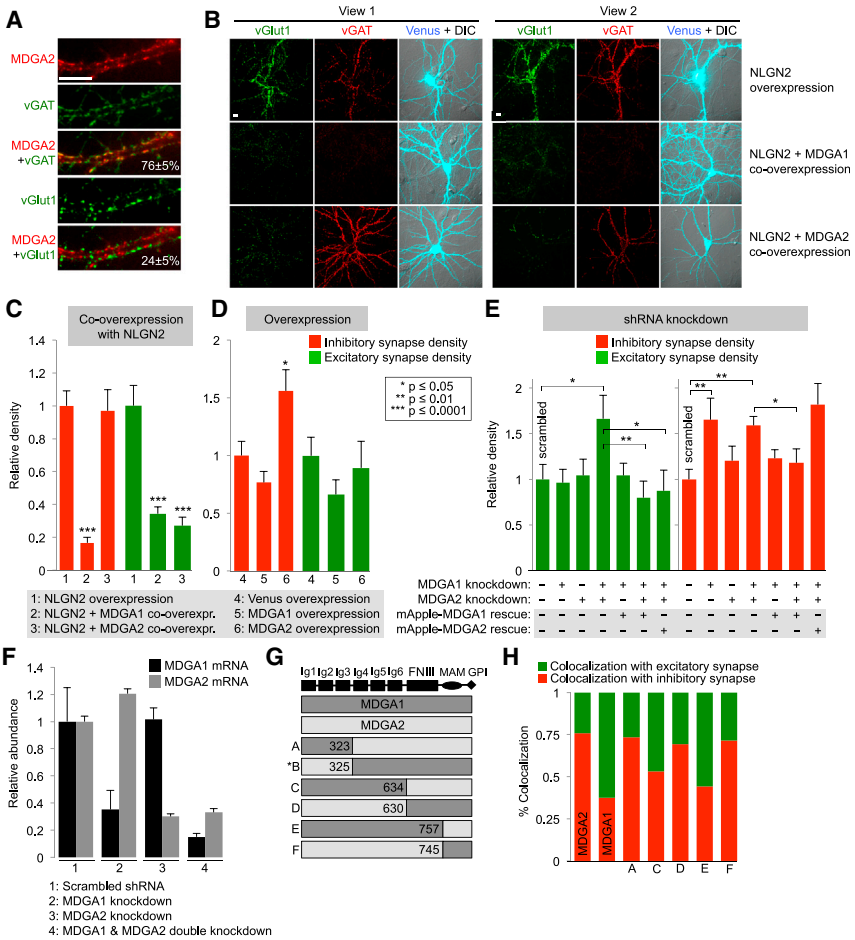

Figure 6. Mdga1 and Mdga2 Have Distinct Synaptic Localizations and Functions

(A) Fluorescence imaging of HRP-Mdga2, via BxxP labeling and neutravidin-AlexaFlour647 staining. Values give colocalization extent with inhibitory (vGAT) and excitatory (vGlut1) synapse markers analyzed from eight fields of view each. Errors, ± 1 SD; scale bar, 10 μm.

(B) Synaptogenesis assay based on overexpression of Nlgn2 to probe specificity of presynaptic vesicle recruitment. Nlgn2 was overexpressed along with Venus fluorescent protein (top), Venus-Mdga1 (middle), or Venus-Mdga2 (bottom). Two fields of view are shown per condition. Enhanced recruitment of excitatory or inhibitory synaptic vesicles to transfected neurons was assessed by staining with anti-vGlut1 and anti-vGAT antibodies, respectively. Images are representative of >20 transfected neurons per condition. Controls show that co-overexpression of Mdga1 or Mdga2 does not alter surface levels of V5-Nlgn2 (data not shown).

(C) Quantitation of data in (B) along with seven additional fields of view per condition. Synapse density is defined as total anti-vGlut1 or anti-vGAT intensity divided by area of transfected neuron. Errors, ± SEM.

(D) Effect of Mdga1 or Mdga2 overexpression (without Nlgn2 co-overexpression) on excitatory and inhibitory vesicle densities, quantified as in (C). 12 fields of view analyzed per condition. Errors, ± SEM.

(E and F) Effect of single or double knockdown of Mdga1 and/or Mdga2 on excitatory and inhibitory vesicle densities (E), quantified as in (C). Knockdowns (from three technical replicates per condition) verified by qPCR in (F) (errors, ± SEM). Representative images in Figure S7D. 15 fields of view analyzed per condition. Errors, ± SEM.

(G) Chimeras of MDGA1 and MDGA2 tested in (H). The parent genes each have six immunoglobulin (Ig) domains, a fibronectin type III (FNIII) domain, a memprin/A5 protein/receptor tyrosine phosphatase mu (MAM) domain, and a C-terminal GPI anchor. Chimera B exhibited poor surface trafficking and was not evaluated further. Numbers refer to amino acid residues at cross-over points.

(H) Relative localization of chimeras to excitatory versus inhibitory synapses, assessed by imaging with anti-vGlut1 and anti-vGAT staining (images and error values shown in Figure S7E). See also Figure S7.

synapse types, while Mdga2 is specifically localized to GABAergic synapses only.

We sought to investigate the hypothesis that Mdga2 has a different function at synapses than Mdga1. Our assay capitalizes on the synaptogenic activity of Nlgn2 (Graf et al., 2004), which when overexpressed on the post-synaptic membrane, over-recruits both vGlut1- and vGAT-positive pre-synaptic terminals (Takahashi et al., 2012) (Figure S7B). When Mdga1 was co-overexpressed with Nlgn2, the enhanced recruitment of both vesicle types was suppressed (Figures 6B and 6C). Co-overexpression of Mdga2, however, suppressed selectively the recruitment of excitatory but not inhibitory vesicles.

Based on these observations, we hypothesized that Mdga1 and 2 both downregulate the *trans*-synaptic vesicle recruiting activity of Nlgn2 (which occurs via unknown presynaptic binding partner[s]) (Figure S7C). However, Mdga1 binds Nlgn2 in such a way that it blocks recruitment of both inhibitory and excitatory vesicles. MDGA2 binds Nlgn2 differently, blocking recruitment of only excitatory vesicles while allowing recruitment of inhibitory vesicles.

To further test this hypothesis, we performed shRNA knockdown of Mdga1, Mdga2, or both together (Figures 6E, 6F, and S7D). The interpretation of the data requires the assumption that each Nlgn2 molecule binds to Mdga1 or 2, but not to both at once. In the case of Mdga1 knockdown, more Nlgn2 is freed to interact with Mdga2 instead. According to our model, Mdga2 promotes inhibitory vesicle recruitment, but not excitatory. Correspondingly, we observe that Mdga1 knockdown causes an increase in inhibitory vesicle signal, but not excitatory signal. This is also consistent with previous observations (Lee et al., 2013; Pettem et al., 2013).

By itself, Mdga2 knockdown had no significant effect, but when combined with Mdga1 knockdown caused both inhibitory and excitatory vesicle signals to increase, consistent with full derepression of Nlgn2 activity. Because this phenotype is distinct from that caused by knockdown of Mdga1 only (increase

in inhibitory vesicle density only), it suggests that Mdga2 plays a role in downregulation of excitatory vesicle recruitment.

We also performed a gain-of-function assay by overexpressing only Mdga1 or Mdga2 (without Nlgn2 co-overexpression) (Figure 6D). More Mdga2 in neurons might shift the equilibrium for Nlgn2, causing more of it to bind to Mdga2 than Mdga1. Accordingly we would expect to see increased inhibitory vesicle recruitment, with no effect on excitatory vesicle recruitment. Our data in Figure 6D shows this expected trend.

Fluorescence imaging of a panel of Mdga1/2 chimeras (Figure 6G) showed that their extracellular juxtamembrane Ig4-6 regions are responsible for their unique synaptic localizations (Figures 6H and S7E). Chimeras with the Ig4-6 region from Mdga1 exhibited "Mdga1-like" localization to both excitatory and inhibitory synapses, while chimeras with the Ig4-6 domain from Mdga2 exhibited "Mdga2-like" localization to inhibitory synapses only. Previous studies have shown that a different region of the Mdgas, the Ig1-3 domain, mediates cis-interactions with Nlgn2 (Lee et al., 2013; Pettem et al., 2013). Therefore, we postulate that the Mdgas target to excitatory and/or inhibitory synapses, governed by their Ig4-6 regions, and independent of interactions with Nlgn2. At inhibitory synapses, each Mdga then interacts with Nlgn2 to differentially regulate its activity. At excitatory synapses, perhaps the role of Mdga1 is to help prevent the invasion of inhibitory synaptic elements (such as pools of Nlgn2 itself) into excitatory terminals.

DISCUSSION

In this study, we develop and extend the APEX platform to achieve successful proteomic mapping of the synaptic cleft. We replace APEX2 with HRP, which is more active at the cell surface, and introduce the BxxP probe for restriction of peroxidase labeling to the neuronal cell surface. We apply an intersectional strategy, using two independent peroxidase fusion constructs targeting the same cellular locale, in order to dramatically improve the specificity of protein identifications. To adapt the technique to primary, non-dividing cells, we employ post-digestion iTRAQ chemical labeling for quantitation, rather than SILAC metabolic labeling, which requires protein turnover. Finally, to overcome background caused by the unique, detergent-insoluble matrix underlying the post-synaptic membrane, we develop a denaturing lysis and streptavidin enrichment procedure that effectively separates intracellular proteins from cleft-exposed transmembrane proteins.

Our study opens the door for APEX to be applied to a greater diversity of cellular structures. This includes other unpurifiable subdomains of the synapse (e.g., the inhibitory post-synaptic region and synaptic ribbons), as well as smaller and more challenging domains across cell biology in general, for example, mitochondria-ER contact sites, RNA granules, the axon initial segment, and even macromolecular complexes. Because peroxidase-catalyzed proteomic tagging occurs in just 1 min (in contrast to BioID which requires 18–24 hr of labeling), it should also be possible to map proteomes under different cell states, such as in response to drugs or LTP, at different synapse maturities, or in models of brain disease.

The excitatory and inhibitory synaptic cleft proteomic lists generated by this study depart from existing synapse proteomes in several respects. First, they are much more specific. Due to contamination by mitochondrial, nuclear (Figures S1A and S1B), and glial proteins, synaptosome and PSD preparations typically have false discovery rates of 20%–40% (Biesemann et al., 2014). This necessitates extensive follow-up experimentation to distinguish genuine synaptic proteins from false positives. By contrast, our datasets have false discovery rates of <10%, or likely much lower, based on our analysis of synapse orphans (Figure 5). Second, our lists have higher coverage (Figure S1C). By tagging in live cells and bypassing detergent lysis and serial centrifugation, we improve protein recovery, enabling us to identify dozens of proteins that were missed by previous synaptosome, PSD, and active zone preparations. These include soluble, secreted proteins such as Gpc6 and Reelin that may dissociate from organelles during centrifugation. Third, our lists chart an important subdomain of the synapse that has eluded previous MS studies because it cannot be purified. Fourth, our lists cleanly separate components of the glutamatergic synapse from components of the GABAergic synapse, in contrast to synaptosome preparations, which blend across all synapse types, and PSD preparations, which are applicable only to excitatory synapses because inhibitory synapses lack a PSD. Biesemann et al. (2014) have attempted to further purify synaptosomes by FACS, but their resulting vGlut1-enriched dataset is imperfect, containing inhibitory synapse components such as Gabrg2, Gabra1, Gabra5, and gephyrin. Here, using the power of genetic targeting, we achieve >98% specificity for excitatory components in our glutamatergic list and >76% specificity for inhibitory components in our GABAergic list (value is corrected based on data shown in Figure S6).

Our inhibitory synapse proteome can also be compared to two previous studies that use immunoprecipitation MS, rather than biochemical fractionation, to identify components of the GABAergic synapse (Heller et al., 2012; Kang et al., 2014). Though the Heller et al. study that uses $GABA_A$ receptor α1 immunoprecipitation is quite specific, both datasets miss the majority of known inhibitory synaptic cleft components (coverage <34%), probably because the baits do not interact directly or stably with these proteins. By contrast, our mapping approach does not require direct interactions, because the biotin-phenoxyl radical diffuses out of the peroxidase active site to tag endogenous proteins in the neighborhood of HRP/APEX.

Both synaptic cleft proteomic lists can be mined for biological insights or hypotheses. We have illustrated this by using our datasets to discover ten synaptic cleft proteins (validated by microscopy and/or synaptosome immunoblotting in Figure 5) and reveal a potential inhibitory synapse component for four known excitatory synaptic cleft proteins (Figure S6). We also followed up on CD200, a protein previously linked to synapses only by crude synaptosome MS data. After observing strong enrichment in our excitatory proteome, we found that CD200 is highly expressed in the visual thalamus during periods of synaptic refinement, and its deletion perturbs the normal development of retinogeniculate synapses.

By also revealing different synaptic sub-type localizations for two known, homologous synaptic proteins (Mdga1 and Mdga2), our proteomic data inspired the hypothesis that these two proteins have different functional roles. Follow-up experiments using gain-of-function and loss-of-function assays in neuron culture suggest that while Mdga1 may act to generally downregulate Nlgn2 activity, Mdga2 may function as a specificity factor at inhibitory synapses to downregulate Nlgn2′s signaling with vGlut1 pre-synaptic terminals, but not vGAT pre-synaptic terminals.

There are many more synapse orphans and synapse subtype orphans identified in our study, on which we did not perform follow-up experimentation. Several of these are intriguing and, if validated, could open up avenues for exploration. For example, Csmd1 is a synapse orphan identified in our inhibitory synaptic cleft proteome. Though no literature describes Csmd1 as a synaptic protein, the CSMD1 gene has been linked by GWAS studies to schizophrenia (Håvik et al., 2011), and the protein may be part of the complement pathway that facilitates synaptic pruning (Hong et al., 2016; Kraus et al., 2006). The detection of endogenous Csmd1 in the inhibitory cleft of live neurons suggests a possible link between inhibitory synapse elimination and schizophrenia that could be explored in future studies. We note that Csmd1 is a very difficult protein to study by conventional techniques, because there are no specific antibodies and recombinant expression via standard techniques is not possible because the protein is enormous (~380 kDa). Proximity biotinylation and MS may be one of the only ways to investigate the subcellular localization of this protein. Interestingly, Csmd1 has been missed in all previous synaptosome, PSD, and active zone purifications.

In conclusion, our study departs from both classical synaptosome and PSD purifications, as well as previous APEX and BioID publications, and demonstrates that peroxidase-based proteomic mapping is a powerful technology for parsing the molecular properties of important nanoscale structures in biology. Mapped with few-nanometer spatial resolution and 1-min temporal resolution, the excitatory and inhibitory synaptic cleft proteomes reported here can serve as rich resources for neuroscientists.

STAR★METHODS

Detailed methods are provided in the online version of this paper and include the following:

SUPPLEMENTAL INFORMATION

Supplemental Information includes seven figures and five tables and can be found with this article online at http://dx.doi.org/10.1016/j.cell.2016.07.041.

AUTHOR CONTRIBUTIONS

K.H.L. performed all experiments except those noted below. K.H.L. and P.S.S. performed shRNA knockdowns. K.H.L. and A.S.D. performed synaptosome purifications, qPCR, and Notch2 imaging in brain slice. N.D.U., T.S., and S.A.C. processed streptavidin-enriched proteomic material and performed mass spectrometry. P.S.S., T.J.D., and M.H.E. performed electron microscopy. E.K.L., D.K.W., and B.S. performed CD200 experiments. K.H.L. and A.Y.T. conceived the study, designed experiments, and analyzed data. K.H.L. and A.Y.T. wrote and revised the manuscript.

ACKNOWLEDGMENTS

We thank N. Watson (Whitehead Institute Keck Microscopy Facility) for performing electron microscopy, J. Einstein for neuron cultures, A. Vignery (Yale) and J. Sedgwick (Schering-Plough) for CD200 knockout mice, and members of A. Ting's lab, especially V. Hung, K. Cox, S. Lam, and K. Pedram, for assistance with data analysis and manuscript editing. K. Tye and G. Matthews assisted with brain slice imaging. J. Sanes, K. Shen, and S. Slavoff provided experimental advice and feedback on the manuscript, and T. Hashimoto helped with data analysis. Funding was provided by the U.S. NIH (R01-CA186568 to A.Y.T.; P41GM103412 and R01GM086197 to M.H.E.; R01-NS071008-01A1 and R01-NS092578 to B.S.) and the Howard Hughes Medical Institute Collaborative Initiative Award (A.Y.T. and S.A.C.) P.S.S. was supported by a Simons Center for the Social Brain Postdoctoral Fellowship and Feodor Lynen Research Fellowship from the Alexander von Humboldt Foundation. The Massachusetts Institute of Technology has filed a patent covering the peroxidase-based proteomic mapping technology. The authors will deposit the genetic constructs used in this work with Addgene (www.addgene.org/).

Received: December 11, 2015
Revised: May 16, 2016
Accepted: July 26, 2016
Published: August 25, 2016

REFERENCES

Allen, N.J., Bennett, M.L., Foo, L.C., Wang, G.X., Chakraborty, C., Smith, S.J., and Barres, B.A. (2012). Astrocyte glypicans 4 and 6 promote formation of excitatory synapses via GluA1 AMPA receptors. Nature *486*, 410–414.

Bayés, A., Collins, M.O., Croning, M.D.R., van de Lagemaat, L.N., Choudhary, J.S., and Grant, S.G.N. (2012). Comparative study of human and mouse postsynaptic proteomes finds high compositional conservation and abundance differences for key synaptic proteins. PLoS One *7*, e46683.

Biesemann, C., Grønborg, M., Luquet, E., Wichert, S.P., Bernard, V., Bungers, S.R., Cooper, B., Varoqueaux, F., Li, L., Byrne, J.A., et al. (2014). Proteomic screening of glutamatergic mouse brain synaptosomes isolated by fluorescence activated sorting. EMBO J. *33*, 157–170.

Boyken, J., Grønborg, M., Riedel, D., Urlaub, H., Jahn, R., and Chua, J.J.E. (2013). Molecular profiling of synaptic vesicle docking sites reveals novel proteins but few differences between glutamatergic and GABAergic synapses. Neuron *78*, 285–297.

Chapman-Smith, A., and Cronan, J.E., Jr. (1999). In vivo enzymatic protein biotinylation. Biomol. Eng. *16*, 119–125.

Chen, J.L., Villa, K.L., Cha, J.W., So, P.T.C., Kubota, Y., and Nedivi, E. (2012). Clustered dynamics of inhibitory synapses and dendritic spines in the adult neocortex. Neuron *74*, 361–373.

Chen, C.-L., Hu, Y., Udeshi, N.D., Lau, T.Y., Wirtz-Peitz, F., He, L., Ting, A.Y., Carr, S.A., and Perrimon, N. (2015). Proteomic mapping in live Drosophila tissues using an engineered ascorbate peroxidase. Proc. Natl. Acad. Sci. U.S.A. *112*, 12093–12098.

Chih, B., Gollan, L., and Scheiffele, P. (2006). Alternative splicing controls selective trans-synaptic interactions of the neuroligin-neurexin complex. Neuron *51*, 171–178.

Graf, E.R., Zhang, X., Jin, S.-X., Linhoff, M.W., and Craig, A.M. (2004). Neurexins induce differentiation of GABA and glutamate postsynaptic specializations via neuroligins. Cell *119*, 1013–1026.

Håvik, B., Le Hellard, S., Rietschel, M., Lybæk, H., Djurovic, S., Mattheisen, M., Mühleisen, T.W., Degenhardt, F., Priebe, L., Maier, W., et al. (2011). The complement control-related genes CSMD1 and CSMD2 associate to schizophrenia. Biol. Psychiatry *70*, 35–42.

Heller, E.A., Zhang, W., Selimi, F., Earnheart, J.C., Ślimak, M.A., Santos-Torres, J., Ibañez-Tallon, I., Aoki, C., Chait, B.T., and Heintz, N. (2012). The biochemical anatomy of cortical inhibitory synapses. PLoS ONE *7*, e39572.

Henn, F.A., Anderson, D.J., and Rustad, D.G. (1976). Glial contamination of synaptosomal fractions. Brain Res. *101*, 341–344.

Hoek, R.M., Ruuls, S.R., Murphy, C.A., Wright, G.J., Goddard, R., Zurawski, S.M., Blom, B., Homola, M.E., Streit, W.J., Brown, M.H., et al. (2000). Down-regulation of the macrophage lineage through interaction with OX2 (CD200). Science *290*, 1768–1771.

Hong, S., Beja-Glasser, V.F., Nfonoyim, B.M., Frouin, A., Li, S., Ramakrishnan, S., Merry, K.M., Shi, Q., Rosenthal, A., Barres, B.A., et al. (2016). Complement and microglia mediate early synapse loss in Alzheimer mouse models. Science *352*, 712–716.

Hung, V., Zou, P., Rhee, H.-W., Udeshi, N.D., Cracan, V., Svinkina, T., Carr, S.A., Mootha, V.K., and Ting, A.Y. (2014). Proteomic mapping of the human mitochondrial intermembrane space in live cells via ratiometric APEX tagging. Mol. Cell *55*, 332–341.

Hung, V., Udeshi, N.D., Lam, S.S., Loh, K.H., Cox, K.J., Pedram, K., Carr, S.A., and Ting, A.Y. (2016). Spatially resolved proteomic mapping in living cells with the engineered peroxidase APEX2. Nat. Protoc. *11*, 456–475.

Kang, Y., Ge, Y., Cassidy, R.M., Lam, V., Luo, L., Moon, K.-M., Lewis, R., Molday, R.S., Wong, R.O.L., Foster, L.J., and Craig, A.M. (2014). A combined transgenic proteomic analysis and regulated trafficking of neuroligin-2. J. Biol. Chem. *289*, 29350–29364.

Kraus, D.M., Elliott, G.S., Chute, H., Horan, T., Pfenninger, K.H., Sanford, S.D., Foster, S., Scully, S., Welcher, A.A., and Holers, V.M. (2006). CSMD1 is a novel multiple domain complement-regulatory protein highly expressed in the central nervous system and epithelial tissues. J. Immunol. *176*, 4419–4430.

Krivosheya, D., Tapia, L., Levinson, J.N., Huang, K., Kang, Y., Hines, R., Ting, A.K., Craig, A.M., Mei, L., Bamji, S.X., and El-Husseini, A. (2008). ErbB4-neuregulin signaling modulates synapse development and dendritic arborization through distinct mechanisms. J. Biol. Chem. *283*, 32944–32956.

Krogh, A., Larsson, B., von Heijne, G., and Sonnhammer, E.L. (2001). Predicting transmembrane protein topology with a hidden Markov model: application to complete genomes. J. Mol. Biol. *305*, 567–580.

Kulik, A., Nakadate, K., Nyíri, G., Notomi, T., Malitschek, B., Bettler, B., and Shigemoto, R. (2002). Distinct localization of GABA(B) receptors relative to synaptic sites in the rat cerebellum and ventrobasal thalamus. Eur. J. Neurosci. *15*, 291–307.

Lam, S.S., Martell, J.D., Kamer, K.J., Deerinck, T.J., Ellisman, M.H., Mootha, V.K., and Ting, A.Y. (2015). Directed evolution of APEX2 for electron microscopy and proximity labeling. Nat. Methods *12*, 51–54.

Lee, K., Kim, Y., Lee, S.-J., Qiang, Y., Lee, D., Lee, H.W., Kim, H., Je, H.S., Südhof, T.C., and Ko, J. (2013). MDGAs interact selectively with neuroligin-2 but not other neuroligins to regulate inhibitory synapse development. Proc. Natl. Acad. Sci. USA *110*, 336–341.

Lerma, J. (2003). Roles and rules of kainate receptors in synaptic transmission. Nat. Rev. Neurosci. *4*, 481–495.

Linhoff, M.W., Laurén, J., Cassidy, R.M., Dobie, F.A., Takahashi, H., Nygaard, H.B., Airaksinen, M.S., Strittmatter, S.M., and Craig, A.M. (2009). An unbiased expression screen for synaptogenic proteins identifies the LRRTM protein family as synaptic organizers. Neuron *61*, 734–749.

Lois, C., Hong, E.J., Pease, S., Brown, E.J., and Baltimore, D. (2002). Germline transmission and tissue-specific expression of transgenes delivered by lentiviral vectors. Science *295*, 868–872.

Martell, J.D., Deerinck, T.J., Sancak, Y., Poulos, T.L., Mootha, V.K., Sosinsky, G.E., Ellisman, M.H., and Ting, A.Y. (2012). Engineered ascorbate peroxidase as a genetically encoded reporter for electron microscopy. Nat. Biotechnol. *30*, 1143–1148.

Matsuda, T., and Cepko, C.L. (2004). Electroporation and RNA interference in the rodent retina in vivo and in vitro. Proc. Natl. Acad. Sci. USA *101*, 16–22.

Pagliarini, D.J., Calvo, S.E., Chang, B., Sheth, S.A., Vafai, S.B., Ong, S.-E., Walford, G.A., Sugiana, C., Boneh, A., Chen, W.K., et al. (2008). A mitochondrial protein compendium elucidates complex I disease biology. Cell *134*, 112–123.

Pettem, K.L., Yokomaku, D., Takahashi, H., Ge, Y., and Craig, A.M. (2013). Interaction between autism-linked MDGAs and neuroligins suppresses inhibitory synapse development. J. Cell Biol. *200*, 321–336.

Pfaffl, M.W. (2001). A new mathematical model for relative quantification in real-time RT-PCR. Nucleic Acids Res. *29*, e45.

Pirooznia, M., Wang, T., Avramopoulos, D., Valle, D., Thomas, G., Huganir, R.L., Goes, F.S., Potash, J.B., and Zandi, P.P. (2012). SynaptomeDB: an ontology-based knowledgebase for synaptic genes. Bioinformatics *28*, 897–899.

Rappsilber, J., Mann, M., and Ishihama, Y. (2007). Protocol for micro-purification, enrichment, pre-fractionation and storage of peptides for proteomics using StageTips. Nat. Protoc. *2*, 1896–1906.

Rees, J.S., Li, X.-W., Perrett, S., Lilley, K.S., and Jackson, A.P. (2015). Selective Proteomic Proximity Labeling Assay Using Tyramide (SPPLAT): A Quantitative Method for the Proteomic Analysis of Localized Membrane-Bound Protein Clusters. Curr. Protoc. Protein Sci. *80*, 19.27.1–19.27.18.

Rhee, H.-W., Zou, P., Udeshi, N.D., Martell, J.D., Mootha, V.K., Carr, S.A., and Ting, A.Y. (2013). Proteomic mapping of mitochondria in living cells via spatially restricted enzymatic tagging. Science *339*, 1328–1331.

Roux, K.J., Kim, D.I., Raida, M., and Burke, B. (2012). A promiscuous biotin ligase fusion protein identifies proximal and interacting proteins in mammalian cells. J. Cell Biol. *196*, 801–810.

Song, J.Y., Ichtchenko, K., Südhof, T.C., and Brose, N. (1999). Neuroligin 1 is a postsynaptic cell-adhesion molecule of excitatory synapses. Proc. Natl. Acad. Sci. USA *96*, 1100–1105.

Svinkina, T., Gu, H., Silva, J.C., Mertins, P., Qiao, J., Fereshetian, S., Jaffe, J.D., Kuhn, E., Udeshi, N.D., and Carr, S.A. (2015). Deep, quantitative coverage of the lysine acetylome using novel anti-acetyl-lysine antibodies and an optimized proteomic workflow. Mol. Cell. Proteomics *14*, 2429–2440.

Takahashi, H., Katayama, K., Sohya, K., Miyamoto, H., Prasad, T., Matsumoto, Y., Ota, M., Yasuda, H., Tsumoto, T., Aruga, J., and Craig, A.M. (2012). Selective control of inhibitory synapse development by Slitrk3-PTPδ trans-synaptic interaction. Nat. Neurosci. *15*, 389–398, S1–S2.

Takamori, S., Holt, M., Stenius, K., Lemke, E.A., Grønborg, M., Riedel, D., Urlaub, H., Schenck, S., Brügger, B., Ringler, P., et al. (2006). Molecular anatomy of a trafficking organelle. Cell *127*, 831–846.

Varoqueaux, F., Jamain, S., and Brose, N. (2004). Neuroligin 2 is exclusively localized to inhibitory synapses. Eur. J. Cell Biol. *83*, 449–456.

STAR★METHODS

KEY RESOURCES TABLE

REAGENT or RESOURCE	SOURCE	IDENTIFIER
Antibodies		
Mouse anti-Bassoon	Enzo Life Sciences	Cat# SAP7F407 RRID: AB_2313990
Mouse anti-vGlut1	UC Davis/NIH NeuromAb	Cat# 75-066 RRID: AB_2187693
Mouse anti-V5	Invitrogen	Cat# R960-25 RRID: AB_2556564
Donkey anti-goat-Alexa-Fluor594	Invitrogen	Cat# A11058 RRID: AB_2534105
Donkey anti-guinea pig-Alexa-Fluor488	Jackson	Cat# 706-545-148 RRID: AB_2340472
Donkey anti-rabbit-Alexa-Fluor647	Invitrogen	Cat# A31573 RRID: AB_2536183
Donkey anti-rabbit-Alexa-Fluor594	Invitrogen	Cat# A21207 RRID: AB_141637
Goat anti-mouse-Alexa-Fluor405	Invitrogen	Cat# A31553 RRID: AB_2536170
Goat anti-mouse-Alexa-Fluor488	Invitrogen	Cat# A11001 RRID: AB_2534069
Goat anti-mouse-Alexa-Fluor568	Invitrogen	Cat# A11004 RRID: AB_2534072
Goat anti-mouse-Alexa-Fluor647	Invitrogen	Cat# A21235 RRID: AB_2535804
Goat anti-rabbit-Alexa-Fluor488	Invitrogen	Cat# A11008 RRID: AB_143165
Goat anti-rabbit-Alexa-Fluor568	Invitrogen	Cat# A11011 RRID: AB_2534078
Goat anti-rabbit-Alexa-Fluor647	Invitrogen	Cat# A21244 RRID: AB_2535812
Goat anti-rabbit-HRP	Bio Rad	Cat# 170-6515 RRID: AB_11125142
Goat anti-mouse-HRP	Bio Rad	Cat# 170-6516 RRID: AB_11125547
Goat anti-CD200	R+D systems	Cat# AF3355 RRID: AB_2073945
Guinea pig anti-VGLUT2	Millipore	Cat# AB2251 RRID: AB_1587626
Mouse anti-GluA1	UC Davis/NIH NeuromAb	Cat# 73-327 RRID: AB_2315839
Rabbit anti-Homer	Synaptic Systems	Cat# 160023
Rabbit anti-vGAT	Synaptic Systems	Cat# 131 013 RRID: AB_1966444
rabbit anti-Tom20	Santa Cruz	Cat# sc-11415 RRID: AB_2207533
Rabbit anti-NeuN	Abcam	Cat# ab104225 RRID: AB_10711153
Rabbit anti-Brinp3	Santa Cruz	Cat# sc-139453 RRID: AB_10840367
Rabbit anti-Sema4a	Abcam	Cat# ab155192
Rabbit anti-Notch2	Abcam	Cat# ab8926 RRID: AB_2267338
Rabbit anti-5HT4 (Tpbg)	Abcam	Cat# ab134162
Rabbit anti-Slc39a10	Novus Biologicals	Cat# NBP1-76507 RRID: AB_11004686
Rabbit anti-Itga6	Abcam	Cat# ab97760 RRID: AB_10680694
Rabbit anti-EGFR	Santa Cruz	Cat# sc-03 RRID: AB_631420
Mouse anti-synaptophysin	Sigma	Cat# S5768 RRID: AB_477523
Mouse anti-PSD95	UC Davis/NIH NeuromAb	Cat# 75-028 RRID: AB_2292909
Mouse anti-beta-actin	Sigma	Cat# A2228 RRID: AB_476697
Chemicals, Peptides, and Recombinant Proteins		
Streptavidin-coated magnetic beads	Pierce	Cat# 88817
Streptavidin-HRP	Thermo Scientific	Cat# 21130
Lipofectamine 2000	Invitrogen	Cat# 11668500
BxxP	This paper	
protease inhibitor cocktail	Sigma	Cat# P8849
Critical Commercial Assays		
RNeasy Mini Kit	QIAGEN	Cat# 74104
Pierce BCA Protein Assay Kit	Thermo Scientific	Cat# 23225
iTRAQ Kit	SciEx	Cat# 4352135

(*Continued on next page*)

Continued		
REAGENT or RESOURCE	SOURCE	IDENTIFIER
Clarity Western ECL Substrate	Bio Rad	Cat# 1705061
Deposited Data		
Mass spec proteomic data	MassIVE	MSV000079849
Experimental Models: Cell Lines		
Human HEK293T cells	ATCC	Cat# CRL-3216
Experimental Models: Organisms/Strains		
Sprague Dawley Rat	Charles River Labs	Strain ID 400
Mouse C57Bl/6J	Jackson Laboratories	RRID:IMSR_JAX:000664
CD200 KO mouse	Generated by Jonathon Sedgwick and kindly gifted to us by Agnes Vignery.	N/A
Recombinant DNA		
See Table S5 for complete list of genetic constructs used in this study	N/A	N/A
Sequence-Based Reagents		
shMDGA1: GTCTCTTTCTTCTACCACA	Lee et al., 2013	N/A
shMDGA2: AGGTGAAGCTAAAGAACAA	Lee et al., 2013	N/A
shScrambl: GATGGTGGCAGTACCAGTG	Pettem et al., 2013	N/A
Please see Table S5 for qPCR primer sequences	N/A	N/A
Software and Algorithms		
Slidebook Version 5.0	Intelligent Imaging Innovations	N/A
Spectrum Mill Version 5.0	Agilent Technologies	N/A
Imaris	Bitplane	N/A
ImageJ	N/A	N/A
Other		
TMHMM database	Krogh et al., 2001	http://www.cbs.dtu.dk/services/TMHMM/
SynaptomeDB database	Pirooznia et al., 2012	http://metamoodics.org/SynaptomeDB/index.php

CONTACT FOR REAGENT AND RESOURCE SHARING

Further information and requests for reagents may be directed to, and will be fulfilled by, the corresponding author Alice Ting (ating@mit.edu or ayting@stanford.edu).

EXPERIMENTAL MODEL DETAILS

Dissociated Rat Neuron Culture

Pregnant wild-type Sprague Dawley rats between 8-10 weeks old were purchased from Charles River Laboratories. After euthanasia by CO_2 asphyxiation, embryos were sacrificed at embryonic day 18 (E18). Dissected rat embryo cortical tissue was digested with papain (Worthington) and DNase I (Roche), then plated onto 0.09–0.12 mm thick glass coverslips (Carolina Biological Supply) in a 1:1 volume ratio of growth medium A and growth medium B and cultured at 37°C under 5% CO_2. Growth medium A is MEM (Sigma) with L-glutamine (Sigma) supplemented with 10% (v/v) fetal bovine serum (GIBCO) and 2% (v/v) B27 (Life Technologies). Growth medium B is Neurobasal medium (Life Technologies) supplemented with 2% (v/v) B27 and 1% (v/v) GlutaMAX (Life Technologies). Glass coverslips were pre-incubated overnight at 37°C with 0.1 mg/mL poly-D-lysine (Sigma) and 3 μg/mL mouse laminin (Life Technologies) in 0.1 M borate buffer. At 4 days in vitro, half of the spent culture medium was replaced with fresh growth medium B in addition to 10 μM 5′-fluoro-2′-deoxyuridine (FUDR, Sigma), an anti-mitotic drug that suppresses growth of glial cells, and replaced similarly every 4 days onward.

Mouse Brain Tissue

For imaging endogenous Notch2, we used brain sections from wild-type adult (6-8 weeks old) male C57Bl/6 mice that were a gift from Kay Tye (MIT). The tissue was fixed by transcardial perfusion of 4% paraformaldehyde (PFA), followed by soaking of dissected tissue

for 5-18 hr in 4% PFA at 4°C. After further soaking in 30% sucrose for 36 hr at 4°C, the brains were sectioned to 30 μm thickness on a freezing microtome (HM430; Thermo Fisher). Sections were stored in PBS at 4°C until antibody staining.

For imaging endogenous CD200, we used wild-type (P5, P10 and P30) (female mice) C57Bl/6 mice obtained from Charles River Laboratories. For analysis of CD200 KO tissue, we used CD200 KO mice, and littermate control wild-type mice, generated by Jonathon Sedgwick (Schering-Plough) (Hoek et al., 2000) and kindly gifted to us by Agnes Vignery (Yale). Mouse experiments were approved by the institutional care and use committee of Boston Children's Hospital in accordance with NIH guidelines for the humane treatment of animals. Brains were harvested from mice following transcardial perfusion with PBS and 4% PFA. Tissue was post-fixed in 4% PFA for two hours after perfusion, and then washed three times with PBS and transferred to 30% sucrose for cryoprotection. Tissue was embedded in a 2:1 mixture of 20% sucrose in PBS: optimal cutting temperature compound (OCT, VWR) and stored at −80°C until use.

HEK293T Cells

Human embryonic kidney (HEK) 293T cells (ATCC) were seeded at 20% confluence in T25 flasks and cultured in Minimum Essential Medium (MEM) supplemented with 10% fetal bovine serum, penicillin, and streptomycin at 37°C under 5% CO_2. Cells were passaged at 80%–90% confluence by trypsinization and reseeded.

METHOD DETAILS

Cloning

Overlap extension PCR was used to clone the four synaptic HRP fusion constructs used for proteomics. We separately PCR-amplified (1) the HRP gene (while introducing a C-terminal V5 tag), (2) the gene for the synaptic adhesion protein of interest, and (3) the native signal sequence for the synaptic adhesion protein. We then joined the three PCR products via PCR overlap extension. The resulting product was digested with restriction enzymes (see "Table of genetic constructs" below for exact restriction sites used), and ligated in-frame into similarly digested FSW vector (for lentivirus generation). The FSW vector was derived from FUGW (Lois et al., 2002), but we replaced the ubiquitin promoter with the human synapsin promoter, and removed the 2A peptide GFP fusion.

Similar strategies were used for also cloning HRP-TM, PSD95-APEX2, and APEX2-NES. The TM region of HRP-TM is PCR-amplified from the commercial pDisplay vector (Invitrogen). For pCAG-V5-NLGN2A, pCAG-Venus-MDGA1 and pCAG-Venus-MDGA2 constructs, we ligated into the pCAG vector (Matsuda and Cepko, 2004) for lipofectamine transduction, instead of the FSW vector, which is for lentivirus generation.

Gibson assembly was used to clone HRP-MDGA1, HRP-MDGA2, MDGA1/2 chimeras, and all synapse orphans tagged with HRP. The FSW-HRP-V5-LRRTM1 plasmid was digested with AgeI and AscI restriction enzymes to remove LRRTM1, and the gene of interest was amplified with primers overlapping with the digested vector.

Lentivirus Preparation and Titration

To prepare lentiviruses, human embryonic kidney (HEK) 293T cells were plated in T25 flasks and cultured in Minimum Essential Medium (MEM) supplemented with 10% fetal bovine serum, penicillin, and streptomycin at 37°C under 5% CO_2. At ~70% confluence (~$2x10^6$ cells), each flask was transfected with 2.25 μg of FSW plasmid, 0.25 μg of VSVG plasmid, and 2.0 μg of dR8.91 plasmid, using 20 μl polyethylenimine (Sigma) in MEM without serum or antibiotics. VSVG and dR8.91 are lentiviral packaging plasmids (Pagliarini et al., 2008). FSW is the transfer plasmid containing the transgene of interest (Lois et al., 2002). Cells were incubated at 37°C for 2-3 hr, then media was replaced with 5 mL of fresh growth media. After 48 hr, the supernatant (containing lentivirus) was collected and filtered through a 0.45 μm syringe filter, flash-frozen with liquid nitrogen and stored at −80°C.

To titrate lentiviruses, frozen aliquots were thawed quickly in a 37°C water bath, then added in various quantities (typically, 1 μl to 200 μL, diluted in growth media to a final volume of 200 μL) to cultured neurons at DIV15. At DIV19, the neurons were labeled and imaged as described below (see "Characterization of peroxidase fusion constructs by microscopy").

The quantity of lentivirus we selected for our experiments was that which gave (1) > 75% infection efficiency, (2) > 2:1 signal-to-noise by fluorescence imaging, and (3) punctate rather than diffuse BxxP labeling patterns. For synapse-localized constructs, we observed a clear transition point at which the BxxP labeling pattern became diffuse rather than punctate (when viral quantities were too high). We selected lentivirus dilutions that gave punctate BxxP staining patterns only.

Synthesis of BxxP Probe

Reagents were purchased from Sigma Aldrich. Biotinamidohexanoyl-6-amino hexanoic acid N-hydroxysuccinimide ester (150 mg, 0.26 mmol) and 36.2 mg (0.263 mmol) tyramine were dissolved in 2.7 mL dimethylsulfoxide (DMSO). 276 μl (1.58 mmol, 6.0 equivalents) of DIPEA (N,N-diisopropylethylamine) was then added, and the reaction was incubated overnight at room temperature with stirring. 15 mL of H_2O was added to quench the reaction, which was then frozen and lyophilized. A brown-white solid mixture remained. 7 mL of cold methanol at −20°C was added drop-wise until the brown solid fully dissolved (the white material remained relatively insoluble at this temperature), then the solution was chilled at −20°C for another 3 hr. The white precipitate was separated using a fritted glass funnel, and washed 4 times with 1 mL ethyl acetate each time. After drying under vacuum, 117 mg (0.20 mmol, 75% yield) of BxxP was obtained as a white solid.

^{1}H-NMR for BxxP (400 MHz, DMSO-d_6): d = 9.17 (s, 1H), 7.89-7.62 (m, 3H), 6.97 (d, ^{3}J = 8.4 Hz, 2H), 6.66 (d, ^{3}J = 8.4 Hz, 2H), 6.43 (s, 1H), 6.37 (s, 1H), 4,36-4.26 (m, 1H), 4.19-4.08 (m, 1H), 3.23-2.89 (m, 6H), 2.81 (dd, ^{2}J = 12.2 Hz, ^{3}J = 5.2 Hz, 1H), 2.75-2.68 (m, 1H), 2.61-2.53 (m, 3H), 2.08-1.96 (m, 6H), 1.66-1.03 (m, 18H) ppm.

MS on an Agilent 6500 series Q-TOF LC/MS: calculated for $C_{30}H_{47}N_5O_5S$ $[M+H]^+$: 590.33; found: 590.327.

Characterization of Peroxidase Fusion Constructs by Microscopy

Fluorescence microscopy was used to characterize both localization and biotinylation activity of peroxidase fusion constructs. At high expression levels, we used anti-V5 staining to detect the peroxidase protein. At low expression levels, however, we found that anti-V5 staining was insufficiently sensitive, so we used biotinylation activity itself (read out by neutravidin-AlexaFluor staining) as a proxy for peroxidase location.

In Figures 1D, 5B, 5D, 6A, S1D, S2A, S4A, S6A-B, S6D, S7A and S7E, HRP fusion constructs were introduced by lentiviral transduction to DIV15 dissociated rat cortical neuron cultures. Four days later, at DIV19, neurons were labeled live with 100 μM membrane-impermeant BxxP and 1 mM H_2O_2 in Tyrode's buffer for 1 min at room temperature. Tyrode's buffer is 145 mM NaCl, 1.25 mM $CaCl_2$, 3 mM KCl, 1.25 mM $MgCl_2$, 0.5 mM NaH_2PO_4, 10 mM glucose, 10 mM HEPES (pH 7.4). After 1 min, the reaction was immediately quenched by replacing the medium with Tyrode's buffer containing 10 mM sodium azide, 10 mM sodium ascorbate, and 5 mM Trolox. The neurons were washed twice more with this quenching buffer, then fixed with 4% paraformaldehyde in "fixation buffer" (60 mM PIPES, 25 mM HEPES, 10 mM EGTA, 2 mM $MgCl_2$, 0.12 M sucrose [pH 7.4]) at room temperature for 10 min. The cells were washed three times with Dulbecco's Phosphate Buffered Saline (DPBS).

To visualize the BxxP labeling sites, the fixed neurons were first blocked with 3% w/v BSA in DPBS for one hour at room temperature, or overnight at 4°C. Then the cells were stained with neutravidin protein (Invitrogen) pre-coupled to AlexaFluor647 (Invitrogen), at 1:1000 dilution, for 1 hr. After three washes with DPBS, the neurons were fixed a second time with membrane permeabilization, to afford antibody access to intracellular targets. Hence, neurons were incubated with 4% paraformaldehyde in "fixation buffer" (see above) for 10 min at room temperature, followed by 0.1% Triton X-100 in DPBS for 7 min at room temperature. After three more washes with DPBS, the cells were blocked with 3% w/v BSA in DPBS for one hour, then stained with antibodies of interest as follows:

- mouse anti-V5 (Invitrogen, 1:1000 dilution)
- mouse anti-Bassoon (Enzo Life Sciences 1:1000 dilution)
- mouse anti-vGlut1 (NeuroMab, 1:1000 dilution)
- rabbit anti-vGAT (Synaptic Systems, 1:1000 dilution)

Each antibody was diluted into 3% w/v BSA in DPBS and incubated with the cells for 2 hr at room temperature. Samples were washed three times with DPBS, then incubated with the secondary antibodies goat anti-mouse AlexaFluor488 and goat anti-rabbit AlexaFluor568 (Invitrogen, 1:1000 dilution each) in 3% w/v BSA in DPBS for one hour. After three more washes in DPBS, neurons were imaged by fluorescence microscopy as described below.

Characterization of Peroxidase Fusion Constructs by Western Blotting

For gel-based visualization of the endogenous proteins biotinylated by peroxidases, we needed to scale up compared to the fluorescence microscopy assays. Two 10 cm dishes were prepared with 2.5M cortical neurons in each. At DIV15, neurons were infected with lentivirus carrying the HRP fusion of interest, using a previously optimized viral dilution. At DIV19, we performed live cell biotinylation using 100 μM BxxP and 1 mM H_2O_2 in Tyrode's Buffer for 1 min at room temperature. The reaction was quenched with three washes of Tyrode's buffer containing 10 mM sodium azide, 10 mM sodium ascorbate, and 5 mM Trolox. After quenching, the neurons were harvested by scraping and pelleted by centrifugation at 3,000 g for 10 min. The supernatant was discarded and the pellet was stored at −80°C overnight.

The cell pellet was lysed by resuspension in 100 μl of 1% SDS lysis buffer (50 mM Tris-HCl, 1% SDS [pH 8.0]) containing protease inhibitor cocktail (Sigma Aldrich, catalog no. P8849), 1 mM PMSF (phenylmethylsulfonyl fluoride), 10 mM sodium azide, 10 mM sodium ascorbate, and 5 mM Trolox. The mixture was boiled for 5 min to denature and separate postsynaptic density proteins, then diluted into 400 μl of 1.25x RIPA lysis buffer to give 1x RIPA lysis buffer (50 mM Tris-HCl [pH] 8.0, 150 mM NaCl, 0.2% SDS, 0.5% sodium deoxycholate, 1% Triton X-100). Lysates were cleared by centrifugation at 16,000 g for 10 min at 4°C.

Lysates were combined with SDS protein loading buffer and boiled for 5 min, before running on an 8% SDS-PAGE gel. The gel was transferred to a nitrocellulose membrane. The membrane was stained with Ponceau S (10 min in 0.1% w/v Ponceau S in 5% (v/v) acetic acid/water) and imaged. After destaining the membrane with deionized water, we blocked it with 3% w/v BSA in TBST (0.1% Tween-20 in Tris-buffered saline) at 4°C overnight. The membrane was rocked in 0.3 μg/mL streptavidin-HRP (Thermo Scientific) in 1% w/v BSA in TBST at room temperature for 1 hr, then washed with TBST four times for 5 min each time. Finally, the blot was developed with Clarity Western ECL Substrate (Bio-Rad) and imaged on an Alpha Innotech gel documentation system.

Fluorescence Microscopy

All fluorescence images except CD200-related ones (described below) were acquired via confocal microscopy on a Zeiss AxioObserver inverted microscope equipped with a Yokogawa spinning disk confocal head, Cascade II:512 camera, and four-color laser launch (405 nm diode, 491 nm DPSS, 561 nm DPSS, and 640 nm diode, all at 50 mW). Images were acquired using Slidebook

software (Intelligent Imaging Innovations), through 40X or 100X oil-immersion objectives, with acquisition times ranging from 300 ms to 1 s. Emission filters were 445/40 nm for AlexaFluor405; 528/38 nm for GFP, Venus and AlexaFluor488; 617/73 nm for AlexaFluor568; and 700/75 for AlexaFluor647.

Neuron images shown in the figures are all z-projections of 5 confocal stacks, each one 0.3 μm apart (spanning 1.5 μm in the z-direction).

For the CD200 tissue images in Figure S6F, we used a Zeiss AxioScan.Z1 instrument running Zen Blue software. The objective was plan-apochromat 25x/0.8M27, the light source was HR diode and HR DPSS, and filters were 420 nm excitation with an emission filter of 525/50 (for AlexaFluor488) and 590 nm excitation with an emission filter of 647/70 (for AlexaFluor594).

For the CD200 super-resolution image in Figure S6G, we used an ELYRA Super-Resolution microscope with Zen software (Carl Zeiss). Lasers used were 561nm, 488nm and 642nm. Objective was alpha-plan-apochromat 100X/1.46 oil. The filters were 488 nm excitation and the beam splitter BP 495-575 + LP 750 (for AlexaFluor488), 561 nm excitation and the beam splitter BP 570-650 + LP 750 (for AlexaFluor594), and 642 nm excitation and the beam splitter LP 655 (for AlexaFluor647).

For the CD200 KO and wild-type tissue images in Figure S6H, we used an LSM 700 confocal microscope running Zen software (Carl Zeiss). Images were acquired with a 63x oil objective, and 488 and 555 nm lasers. Emission filters were BP 490-555 (for AlexaFluor488) and LP 650 (for AlexaFluor594). Orthogonal image was created with Imaris software (Bitplane).

Electron Microscopy

For EM, neurons were plated onto (laminin and poly-D-lysine-coated) 35 mm glass bottom dishes (MatTek) instead of regular culture dishes. HRP fusions were introduced by lentiviral transduction as described above, at DIV15, then fixed for EM at DIV19. For fixation, 2% glutaraldehyde (Electron Microscopy Sciences) in sodium cacodylate buffer (100 mM sodium cacodylate with 2 mM $CaCl_2$ [pH 7.4]), pre-warmed to 37°C, was added to each sample. This was then removed immediately and fresh fixative was added again. Cells were moved to ice and incubated for 1 hr. All subsequent steps through uranyl acetate staining took place on ice and with pre-chilled solutions. After fixation, samples were washed 5 × 2 min with cold sodium cacodylate buffer, then quenched with 20 mM glycine in sodium cacodylate buffer for 5 min. Cells were rinsed again with cold sodium cacodylate buffer for 5 × 2 min. The samples were then reacted with a solution of 1.4 mM 3,3′-diaminobenzidine (DAB) and 1 mM H_2O_2 in cold sodium cacodylate buffer, for between 30 min and 1 hr, depending on the construct. A guideline is that a faint brown color became visible to the naked eye when the DAB reaction had progressed. To stop the reaction, the cells were rinsed 5 × 2 min with cold sodium cacodylate buffer.

The DAB polymers were subsequently stained with reduced 1% OsO_4 (R-OTO) for 2 hr in cold sodium cacodylate buffer. R-OTO was made by mixing 2% potassium ferrocyanide (Allfa Aesar) in sodium cacodylate buffer with 2% OsO_4 (Electron Microscopy Sciences) and chilling to 4°C. Samples were rinsed 5 × 2 min in chilled Millipore water. Cold 2% aqueous uranyl acetate (Electron Microscopy Sciences) was then added, and the samples were incubated overnight at 4°C.

The samples were rinsed 5 × 2 min with distilled water, then dehydrated progressively, for 2 min each, in 20% ethanol, 50% ethanol, 70% ethanol, 90% ethanol, 95% ethanol, 100% ethanol at 4°C, and 100% ethanol at room temperature. Samples were infiltrated for 30 min in Durcupan ACM resin (Sigma Aldrich) using 1:1 (v/v) resin and anhydrous ethanol for 30 min, then 4 exchanges of 100% resin for 1-2 hr each. After infiltration, the samples were polymerized for 48 hr at 60°C. The DAB-stained areas of the embedded cell samples were identified by transmitted light, selectively sawed out using a jeweler's saw and mounted on dummy acrylic blocks with cyanoacrylic adhesive (Krazy Glue, Elmer's Products). The coverslip was removed, the block trimmed, and cut into ultrathin 80 nm sections using a diamond knife on a Leica Ultracut UCT. Sections were mounted on graphene-covered copper grids and imaged either at the Whitehead Institute Keck Microscopy Facility on a FEI Tecnai G^2 Spirit BioTWIN transmission electron microscope operating at 80 keV (this applies to HRP-SLITRK3 of Figures 1F and S2C) or at UCSD on a JEOL 1200 transmission electron microscope operating at 80 keV (HRP-LRRTM1, HRP-LRRTM2, and HRP-NLG2A of Figures 1F and S2C).

qPCR Analysis of Peroxidase mRNA Levels

Neuron samples were cultured in 6-well (9.5 cm^2/well) dishes containing ~300,000 neurons per well. Each plate was infected with lentiviruses containing the peroxidase constructs of interest, at DIV14. At DIV19, cells were scraped, lysed, and RNA-extracted using an RNeasy Mini Kit (QIAGEN). Total RNA was primed with random hexamers, then transcribed into cDNA using SuperScript III Reverse Transcriptase (Invitrogen). Standard conditions were used: 25°C annealing temperature for 10 min, 50°C transcription temperature for 50 min; and 85°C termination temperature for 10 min. qPCR was then performed on an ABI Stepone qPCR system using SYBR green chemistry (ThermoFisher). Each target primer set was designed to anneal to both the human and rat loci. The efficiency of each primer set was measured from a standard dilution curve of cDNA generated from cultured rat cortical neurons at DIV19 plotted against the threshold cycle C_t. This efficiency was taken into account when quantifying relative mRNA levels. Relative expression levels were measured using the Pfaffl method (Pfaffl, 2001) with housekeeping gene GAPDH as the reference gene. qPCR primer sequences are given in Table S5, Tab 2.

Western Blot Analysis of HRP-Nlgn2 Extent of Overexpression

Neurons infected, labeled, and harvested as described above ("Characterization of peroxidase fusion constructs by western blotting") were lysed in 1x RIPA lysis buffer and boiled in SDS protein loading buffer for 5 min, before running on an 8% SDS-PAGE gel. The gel was transferred to a nitrocellulose membrane, blocked in 3% BSA TBST and immunoblotted with mouse anti-Nlgn2

(synaptic systems 1:2000) in 1% w/v BSA in 1x TBST at room temperature for 1 hr, then washed with 1x TBST four times for 5 min each time. The blot was probed with goat anti-mouse HRP conjugate (1:3000) for 1 hr, then washed with 1x TBST four times for 5 min each time. Finally, the blot was developed with Clarity Western ECL Substrate (Bio-Rad) and imaged on an Alpha Innotech gel documentation system.

Optimization of Neuron Lysis and Streptavidin Enrichment

The optimized conditions (condition 2 in Figure 2D) used for proteomics were as follows. After infection, BxxP labeling, and generation of cell pellets as described above ("Characterization of peroxidase fusion constructs by western blotting"), we lysed each pellet in 100 μl of 1% SDS lysis buffer: 1% SDS in 50 mM Tris (pH 8) containing protease inhibitor cocktail (Sigma Aldrich, catalog no. P8849), 1 mM PMSF, 10 mM sodium azide, 10 mM sodium ascorbate, and 5 mM Trolox. The samples were boiled at 95°C for 10 min, then diluted into 400 μl of 1.25X RIPA lysis buffer to give 1x RIPA lysis buffer (50 mM Tris-HCl [pH 8.0], 150 mM NaCl, 0.2% SDS, 0.5% sodium deoxycholate, 1% Triton X-100).

The lysates were cleared by centrifugation at 16,000 g for 10 min at 4°C, then 150 μl of streptavidin magnetic bead slurry (Pierce), which had been washed twice with RIPA lysis buffer, was added to each sample, and incubated overnight at 4°C with gentle rotation. Beads were then washed with 2 × 1 mL RIPA lysis buffer, 1 × 1 mL of 1M KCl, 1x 1 mL of 0.1 M Na_2CO_3, 1 × 1 mL of 2 M urea in 10 mM Tris-HCl (pH 8.0), and again with 2 × 1 mL RIPA lysis buffer. To elute the biotinylated proteins, we boiled the beads for 10 min in 50 μl of 3x protein loading buffer supplemented with 20 mM dithiothreitol DTT and 2 mM biotin. The streptavidin eluate was collected and run on an 8% SDS-PAGE gel.

The alternative lysis/streptavidin enrichment conditions in Figure 2D (conditions 1, 3, and 4) had the following modifications from the above. For conditions 1 and 3, we used a non-denaturing RIPA lysis, which consisted of resuspending each cell pellet in 1x RIPA lysis buffer (50 mM Tris-HCl [pH 8.0], 150 mM NaCl, 0.2% SDS, 0.5% sodium deoxycholate, 1% Triton X-100) containing protease inhibitor cocktail (Sigma Aldrich, catalog no. P8849), 1 mM PMSF, 10 mM sodium azide, 10 mM sodium ascorbate, and 5 mM Trolox, and incubating on ice for 30 min. For conditions 3 and 4, the streptavidin bead washing was slightly modified to include an additional wash with 4M urea in 10 mM Tris-HCl (pH 8.0], following the 2M urea wash.

To analyze the streptavidin eluates in Figure 2D, we ran the samples on 8% SDS-PAGE gel and transferred to nitrocellulose as described above. After blocking the nitrocellulose membrane with 3% w/v BSA in 1x TBST at 4°C overnight, we stained with antibodies as follows:

- mouse anti-GluA1 (NeuromAb, 1:1000 dilution)
- rabbit anti-Homer (Synaptic Systems, 1:1000 dilution)
- mouse anti-V5 (Invitrogen, 1:1000 dilution)
- mouse anti-PSD95 (NeuromAb, 1:1000 dilution)

Each antibody was diluted into 1% w/v BSA in 1x TBST, and incubated with the nitrocellulose membrane at room temperature for 1 hr. The membrane was then washed 5 × 5 min with 1x TBST, and incubated with secondary goat anti-mouse HRP conjugate (1:3000 dilution) or goat anti-rabbit HRP conjugate (1:3000 dilution) for 1 hr, then washed 4 × 5 min with 1x TBST. Finally, the blot was developed with Clarity Western ECL Substrate (Bio-Rad) and imaged on an Alpha Innotech gel documentation system.

Proteomic Labeling and Mass Spectrometry

Biotinylation and Streptavidin Enrichment

12 individual samples were prepared as shown in Figure 3A. For each sample, we cultured 15 million cortical neurons in six 10-cm dishes. Neurons were infected with lentivirus carrying the appropriate HRP fusion gene at DIV15 using previously optimized quantities. To ensure even virus distribution across six dishes, we pre-diluted virus into 6 mL of neurobasal medium, then added 1 mL per dish. At DIV19, we labeled the neurons live with 100 μM BxxP and 1 mM H_2O_2 in Tyrode's buffer for 1 min at room temperature. Labeling was quenched after 1 min by replacing the media with a quencher solution consisting of Tyrode's buffer with 10 mM sodium azide (VWR), 10 mM sodium ascorbate (VWR), and 5 mM Trolox (Sigma). We used the quencher solution to wash the neurons 3 more times. Then neurons were then harvested by scraping. A small fraction of each sample (~2.5%) was separated for BCA protein concentration analysis (Pierce, see below). For the remainder, the neurons were pelleted by centrifugation at 3,000 g for 10 min. The supernatant was discarded and the pellet was stored at −80°C overnight. These steps were performed independently for the 12 different proteomic samples. Hence, the result was 12 individual cell pellets.

Each cell pellet was lysed by resuspension in 400 μl of 1% SDS in 50 mM Tris-HCl (pH 8.0) containing protease inhibitor cocktail (Sigma Aldrich, catalog no. P8849), 1 mM PMSF, 10 mM sodium azide, 10 mM sodium ascorbate, and 5 mM Trolox. The sample was then boiled for 5 min to dissociate the PSD, and diluted into 1600 μl of 1.25x RIPA lysis buffer (50 mM Tris-HCl, 187.5 mM NaCl, 0.625% sodium deoxycholate, 1.25% Triton X-100) to give 1x RIPA lysis buffer (50 mM Tris-HCl [pH 8.0], 150 mM NaCl, 0.2% SDS, 0.5% sodium deoxycholate, 1% Triton X-100). Lysates were cleared by centrifugation at 16,000 g for 10 min at 4°C.

To measure protein concentrations using the BCA kit (Pierce), we used the ~2.5% of material set aside previously, not the lysate above. This is because the sodium azide, ascorbate, and Trolox that we add to our large-scale lysis buffer interferes with the BCA kit. Thus, we took the ~2.5% neuron material for each sample, and lysed the neurons in the identical lysis buffer *without* sodium azide, ascorbate, and Trolox. BSA was used as the reference standard for this concentration measurement.

Streptavidin-coated magnetic beads (Pierce catalog no. 88817) were prepared by washing twice with RIPA lysis buffer. For each lysed sample, 7.0 mg of total protein was incubated with 450 μl of streptavidin bead slurry overnight at 4°C with gentle rotation. The beads were washed with 2 × 1 mL RIPA lysis buffer, 1 mL of 1 M KCl, 1 mL of 0.1 M Na_2CO_3, 1 mL of 2 M urea in 10 mM Tris-HCl (pH 8.0), and again with 2 × 1 mL RIPA lysis buffer. Finally the beads were resuspended in 1 mL of RIPA lysis buffer before on bead digestion.

As a quality control measure, to check that the streptavidin enrichment of biotinylated proteins worked, we took a small fraction of the beads, and eluted the proteins by boiling for 10 min in 50 μl of 3x protein loading buffer supplemented with 20 mM dithiothreitol DTT and 2 mM biotin, as described above ("Optimization of neuron lysis and streptavidin enrichment"). The supernatants were loaded onto 8% SDS-PAGE, and visualized by silver stain (Pierce). We checked for more eluted protein from experimental samples than from negative controls (no peroxidase, or H_2O_2 omitted, for example), as shown in Figure 2B.

On-Bead Trypsin Digestion

Proteins bound to streptavidin beads were washed with 2 × 200 μl of 50 mM Tris (pH 7.5), followed by 2 × 200 μl of 2 M urea/50 mM Tris (pH 7.5). All buffer was removed, and then beads were resuspended in 80 μl of 2 M urea/50 mM Tris (pH 7.5)containing 1 mM DTT and 0.4 μg trypsin. Beads were incubated with trypsin for 1 hr at 25°C while shaking at 1000 rpm. Afterward, the supernatant was removed transferred to a fresh tube. The streptavidin beads were washed again with 2 × 60 μl of 2 M urea/50 mM Tris (pH 7.5), and the washes were combined with the on-bead digest supernatant. The eluate was reduced with 4 mM DTT (final concentration) for 30 min at 25°C with shaking at 1000 rpm. The samples were alkylated with 10 mM iodoacetamide and incubated for 45 min in the dark at 25°C while shaking (1000 rpm). An additional 0.5 μg of trypsin was added to the sample and the digestion was completed overnight at 25°C with shaking at 700 rpm. After overnight digestion, the sample was acidified to pH < 3 by adding formic acid (FA) to a final concentration of ~1% FA. Samples were desalted on C18 stage tips and evaporated to dryness in a vacuum concentrator.

iTRAQ Labeling of Peptides

Desalted peptides were labeled with iTRAQ (4-plex) reagents as directed by the manufacturer (Sciex, Foster City, CA). Peptides were resuspended in 30 μl dissolution buffer and 70 μl ethanol. One unit of iTRAQ labeling reagent was used for each condition in a given iTRAQ 4-plex cassette according to the scheme shown in Figure 3A. Samples were incubated with iTRAQ reagents for 1 hr at room temperature. iTRAQ labeling reactions were quenched with 10 μl of 1 M Tris (pH 8). Differentially labeled peptides were mixed to generate 4-plex iTRAQ samples, desalted on C18 Stagetips and evaporated to dryness in a vacuum concentrator.

Fractionation of Peptides

For each iTRAQ 4-plex cassette, 50% of the sample was fractionated by Strong Cation Exchange (SCX) using StageTips (Rappsilber et al., 2007) while the other 50% of each sample was reserved for LC-MS analysis by a single-shot, long gradient. One SCX StageTip was prepared per sample using 3 plugs of SCX material (3M, catalog #2251) topped with 2 plugs of C18 material (3M, catalog #2215). StageTips were washed with 100 μl methanol, then with 100 μl 80% acetonitrile/0.5% acetic acid, and equilibrated with 100 μl 0.5% acetic acid. Samples were reconstituted in 0.5% acetic acid, loaded onto the StageTip and then trans-eluted from the C18 discs to the SCX discs using 100 μl of 80% acetonitrile/0.5% acetic acid. Three stepwise elutions from the SCX disks were completed as follows: the first fraction was eluted with 50 μl of 50 mM NH_4AcO; 20% MeCN (pH 5.15, adjusted with acetic acid), the second with 50 μl 50 mM NH_4AcO; 20% MeCN (pH 8.25, adjusted with acetic acid), and the third with 50 μl 50 mM NH_4AcO; 20% MeCN (pH 10.3, adjusted with acetic acid). Each eluate was collected separately and 200 μl of 0.5% acetic acid was added to each. Each fraction was desalted on C18 StageTips and evaporated to dryness in a vacuum concentrator.

Liquid Chromatography and Mass Spectrometry

Desalted, iTRAQ-labeled peptides were resuspended in 9 μl of 3% MeCN, 0.1% FA and analyzed by online nanoflow liquid chromatography tandem mass spectrometry (LC-MS/MS) using a Q-Exactive mass spectrometer (Thermo Fisher Scientific) coupled on-line to a Proxeon Easy-nLC 1000 (Thermo Fisher Scientific). Four microliters of each sample was loaded at 500 nL/minute onto a microcapillary column (360 μm outer diameter × 75 μm inner diameter) containing an integrated electrospray emitter tip (10 μm), packed to approximately 24 cm with ReproSil-Pur C18-AQ 1.9 μm beads (Dr. Maisch GmbH) and heated to 50°C. The HPLC solvent A was 3% MeCN, 0.1% FA, and the solvent B was 90% MeCN, 0.1% FA. Peptides were eluted into the mass spectrometer at a flow rate of 200 nL/minute. SCX fractionated samples were run using a 150 min inject-to-inject LC-MS method, using the gradient previously described (Svinkina et al., 2015). For single-shot, long runs, a 290 min inject-to-inject LC-MS/MS method was utilized. For the 290 min method, after a 1 min ramp to 6% B, a gradient of 0.1% B/minute was applied for 234 min followed by a ramp to 60% B (3.3% B/minute). The Q Exactive was operated in the data-dependent mode acquiring HCD MS/MS scans (r = 17,500) after each MS1 scan (r = 70,000) on the top 12 most abundant ions using an MS1 target of 3×10^6 and an MS2 target of 5×10^4. The maximum ion time utilized for MS/MS scans was 120 ms; the HCD-normalized collision energy was set to 28; the dynamic exclusion time was set to 20 s, and the peptide match and isotope exclusion functions were enabled. Charge exclusion was enabled for charge states that were unassigned, 1 and > 7.

Analysis of Proteomic Data

Initial Data Cleanup

All MS data were interpreted using the Spectrum Mill software package v5.0 pre-release (Agilent Technologies, Santa Clara, CA). Similar MS/MS spectra acquired on the same precursor m/z within ± 60 s were merged. MS/MS spectra were excluded

from searching if they failed the quality filter by not having a sequence tag length > 0 or did not have a precursor MH^+ in the range of 750-4000. MS/MS spectra were searched against a UniProt database containing 29,055 rat proteins and < 200 common laboratory contaminants. All spectra were allowed ± 20 ppm mass tolerance for precursor and product ions, 30% minimum matched peak intensity, and trypsin allow P enzyme specificity with up to 4 missed cleavages. Carbamidomethylation at cysteine and iTRAQ at N-termini and lysine were fixed modifications. Allowed variable modifications were oxidized methionine and N-terminal protein acetylation. Individual spectra were automatically designated as confidently assigned using the Spectrum Mill autovalidation module. Specifically, a target-decoy based false discovery rate (FDR) scoring threshold criteria via a two-step auto threshold strategy at the spectral and protein levels was used. First, peptide mode was set to allow automatic variable range precursor mass filtering with score thresholds optimized to yield a spectral level FDR of < 1.2%. A protein polishing autovalidation was applied to further filter the peptide spectrum matches using a target protein-level FDR threshold of 0.

Each of the three iTRAQ experiments was analyzed separately. Contaminants and proteins identified as reverse hits were removed. For each experiment, only proteins with two or more unique quantified peptides were considered "detected" and retained for further analysis. Unique peptides are those that are designated by SpectrumMill software as peptides not shared with other protein groups.

To normalize the proteomic data, we examined a subset of proteins we expect *not* to be biotinylated by HRP + BxxP: intracellular mitochondrial proteins. We identified these proteins by their presence in our False Positive FP1 list (Table S4, Tab 5), and by their "mitochondria" annotation in Column E of this FP1 list (there are 562 such proteins in FP1; the generation of FP1 list is described in the following section). We then normalized all iTRAQ ratios in each dataset such that the median $\log_2$114/117, $\log_2$115/117 and $\log_2$116/117 = 1 for the mitochondrial subset of proteins. Data provided in Table S4, Tab 1-3 are already normalized in this way.

Removal of Non-biotinylated Proteins, Filter 1

For each detected protein (Table S4, Tabs 1-3), its 114/117 or 115/117 iTRAQ ratio is a measure of its extent of biotinylation by excitatory synapse-localized HRP or inhibitory synapse-localized HRP, respectively. High 114/117 iTRAQ ratio in Experiment 1 reflects high likelihood of biotinylation by HRP-LRRTM1, for example, whereas low 114/117 iTRAQ ratio reflects likelihood of being merely a non-specific binder to streptavidin beads. To determine the 114/117 iTRAQ ratio cut-off above which we would retain proteins, and below which we would exclude them, we classified all proteins detected in each experiment into three groups: (1) true positives, based on the TP1 list in Table S4, Tab 4 that contains 176 known synaptic proteins, (2) false positives, based on the FP1 list in Table S4, Tab 5 that contains likely intracellular proteins that should be inaccessible to the BxxP radical*, and (3) all other proteins. The iTRAQ ratios of proteins in groups 1 and 2 were plotted in histograms such as Figure 3C. Six such histograms were generated: for the three experiments, and two iTRAQ ratios per experiment (114/117 and 115/117).

*To generate the FP1 list, we searched GOCC for all human proteins with the following annotations: nucleus, mitochondria, peroxisome, lysosome, cytosol, endoplasmic reticulum, and Golgi. From this collection, we then removed proteins with "extracellular" annotation in GOCC, proteins present in the TP1 list, and proteins enriched in previous synapse studies by Bayés et al., 2012, Biesemann et al., 2014, Boyken et al., 2013, and Pirooznia et al., 2012. Note that this list may contain a small number of surface-exposed proteins, because GOCC is incomplete, and we did not manually curate this list via literature searches.

We used receiver operating characteristic (ROC) curves to determine the iTRAQ ratio cutoffs that would maximize the retention of true positives while minimizing the retention of false positives in each case, as described in detail in (Hung et al., 2016). The optimized "Filter 1" cut-offs applied to the data were:

Experiment 1 excitatory ($\log_2$(114/117)) cut-off: 0.875
Experiment 1 inhibitory ($\log_2$(115/117)) cut-off: 0.540
Experiment 2 excitatory ($\log_2$(114/117)) cut-off: 0.774
Experiment 2 inhibitory ($\log_2$(115/117)) cut-off: 0.545
Experiment 3 excitatory ($\log_2$(114/117)) cut-off: 0.862
Experiment 3 inhibitory ($\log_2$(115/117)) cut-off: 0.835

Removal of Non-proximal Proteins, Filter 2

The second filter applied to the data was for the purpose of enriching synaptic over non-synaptic cell surface proteins. Here, we used the 114/116 and 115/116 iTRAQ ratios as a measure of relative proximity to synaptic HRP versus general cell surface HRP-TM. Again, we sorted all proteins from Table S4, Tabs 1-3 into three groups: (1) true positives, based on the TP1 list in Table S4, Tab 4 that contains 176 known synaptic proteins, (2) false positives, based on the FP2 list in Table S4, Tab 6 that contains *non*-synaptic cell surface proteins*, and (3) all other proteins. The iTRAQ ratios of proteins in groups 1 and 2 were plotted in histograms such as Figure 3D. Six such histograms were generated: for the three experiments, and two iTRAQ ratios per experiment (114/116 and 115/116).

*To generate the FP2 list in Table S4, Tab 6, we searched GOCC for the following annotations: cell surface, extracellular space, extracellular region, external side of plasma membrane, extracellular matrix, extracellular vesicular, integral component of plasma membrane. From this collection, we then removed proteins with "mitochond" annotation in GOCC, proteins present in the TP1 or FP1 lists, and proteins enriched in previous synapse studies by Bayés et al., 2012, Biesemann et al., 2014, Boyken et al., 2013, and Pirooznia et al., 2012.

We used receiver operating characteristic (ROC) curves to determine the iTRAQ ratio cutoffs that would maximize the retention of true positives (synaptic proteins) while minimizing the retention of false positives (non-synaptic cell surface proteins) in each case, as

described in detail in (Hung et al., 2016). However, here we applied a weight to the FPR, to account for the fact that our FP2 list will inadvertently include some synaptic proteins. This weight was 0.8446, which is equal to the number of proteins in FP2 (2414 proteins), divided by the total number of cell surface proteins identified by GOCC searching (2858 rat proteins; this includes proteins that have synapse annotation). This number is an estimate of the probability that any particular protein in FP2 is non-synaptic. Our optimized "Filter 2" cut-offs that maximize [TPR - 0.8446 × FPR] were:

Experiment 1 excitatory (log_2(114/116)) cut-off: 0.435
Experiment 1 inhibitory (log_2(115/116)) cut-off: −0.144
Experiment 2 excitatory (log_2(114/116)) cut-off: 0.443
Experiment 2 inhibitory (log_2(115/116)) cut-off: 0.033
Experiment 3 excitatory (log_2(114/116)) cut-off: 0.366
Experiment 3 inhibitory (log_2(115/116)) cut-off: 0.215

Filtering Data by E/I Ratio, Filter 3

The purpose of our final filter was to remove proteins strongly enriched by excitatory synapse HRP over inhibitory synapse HRP from our inhibitory synaptic cleft proteome, and vice versa. To do this, we made use of the 114/115 (E/I) iTRAQ ratios, which we averaged for each protein across the three independent experiments (values shown in Column Q of Table S1, Tab 1-2). We then subdivided the True Positive protein list TP1 into 54 exclusively excitatory proteins (those annotated "E" in Column A of Table S3, Tab 1), and 16 exclusively inhibitory proteins (those annotated "I" in Column A of Table S3, Tab 2) (based on prior literature evidence).

We selected E/I cut-offs for the excitatory and inhibitory synaptic cleft proteomes based on False Discovery Rates, or FDRs, calculated as follows. For the excitatory proteome, we calculated FDR as a function of E/I ratio as:

$$FDR\,(E/I\ ratio) = P\,(E/I\ ratio\,|\,(inhibitory))/P(E/I\ ratio\,|\,(excitatory))$$

The numerator is the conditional probability of finding an inhibitory synaptic protein (a false positive) above a given E/I cut-off, and the denominator is the conditional probability of finding an excitatory synaptic protein (a true positive), above the same E/I cut-off. We selected an E/I cut-off (average log_2(114/115) = −0.243) that gave an FDR of 0.2. Proteins with E/I ratio above this cut-off are 5 times more likely to be excitatory than inhibitory. The E/I cut-off (average log_2(114/115) = 0.484) for the inhibitory synaptic cleft proteome was calculated analogously, also to give an FDR of < 0.2 for the inhibitory dataset.

Calculation of Synapse Specificity, Related to Figure 4B

Synapse specificity was calculated as the fraction of proteins in each proteome with prior synapse annotation (Table S1, Tabs 1-2, Column R). We searched the following for prior synapse annotation: our True Positive protein lists TP1 (Table S4, Tab 4); a MS study of fractionated cortex post-synaptic densities (Table S1 of Bayés et al., 2012) (Columns S,T and U of our Table S1, Tabs 1-2); a MS study of purified synaptosomes (Tables S1 and S2 of Biesemann et al., 2014) (Columns W and X); a MS study of presynaptic vesicle docking complexes (Table S1 of Boyken et al., 2013) (Column V); the bioinformatics database Synaptome DB (Pirooznia et al., 2012) (Columns Y-AB); literature demonstrating synaptic localization by imaging or biochemical fractionation (Column AI); and literature showing a functional relationship to synapses (Columns AE and AD). A "1" in any of these columns indicates that a protein is synaptic and is counted toward the synapse specificity.

To calculate the synapse specificity of the entire rat proteome (Figure 4B, column 1), we retrieved the entire rat proteome, 38,912 proteins, from the Uniprot-GO Annotation database in July 2015, and calculated the fraction of Uniprot IDs with the annotation "synapse" (445 proteins).

Calculation of Synapse Subtype Specificity, Related to Figure 4B

To calculate the synapse subtype specificities of the excitatory and inhibitory synaptic cleft proteomes (columns 4 and 5 of Figure 4B), we searched the literature for references identifying each protein in the respective synapse type (see Table S1, Tab 1-2, columns AK-AL). Additionally, we searched MS data generated from vGlut1-sorted synaptosomes (Table S2 of Biesemann et al., 2014), and immunoprecipitation data from inhibitory synapse studies (Heller et al., 2012; Kang et al., 2014).

Calculation of Depth of Coverage

To calculate coverage, we subdivided our True Positive protein list TP1 into excitatory-specific and inhibitory-specific true positive lists, TP2 and TP3, respectively (Table S3, Tabs 1-2). Note that many proteins in TP1 could not be assigned into TP2 or TP3, because synapse subtype specificity information is not available – these include proteins identified via synaptosome purifications, or characterized via EM imaging only, for example.

Analysis of Sub-synaptic Localization of Proteomic Hits, Related to Figure 4B

The sub-synaptic localization of each protein (Columns 6 and 7 of Figure 4B and Table S1, Tab 1-2, column AM) was assigned on the basis of: GOCC; individual references; sub-synaptic localization given in SynaptomeDB (Pirooznia et al., 2012); and identification in Bayés et al., 2012 PSD proteome.

Imaging of HRP-Tagged Synapse Orphans

Rat cortical neuron cultures were infected at DIV15 with lentivirus carrying the construct of interest. For many of the orphans, it was necessary to use very dilute virus in order to achieve punctate labeling patterns. For example, we tested 10 – 0.1 μl of lentivirus harvested from a T25 flask, and incubated with 2 mL of media for 48 hr, at a MOI < <1. At DIV19, the lentivirus-infected

neurons were labeled live with BxxP, fixed, and stained as described above ("Characterization of peroxidase fusion constructs by microscopy").

Synaptosome Purification and Western Blotting

We purified synaptosomes from adult wild-type rat brain according to the protocol of Linhoff et al., 2009. All steps were performed at 4°C. One adult rat brain was homogenized using a Dounce homogenizer in five volumes of Buffer 1 (5 mM HEPES [pH 7.4], 1 mM $MgCl_2$, 0.5 mM $CaCl_2$, 1 mM DTT, 0.32 M sucrose, supplemented with protease inhibitors. This suspension, called the "Homogenate" fraction, or "H" in Figure 5F, was cleared by centrifugation for 10 min at 1400 g, and the supernatant was set aside. The pellet was resuspended in 20 mL Buffer 1, and the suspension was cleared again by centrifugation for 10 min at 710 g. The supernatant was pooled with the supernatant collected after the first centrifugation, and labeled fraction "S1." S1 was fractionated further by another round of centrifugation for 10 min at 13,800 g, and the supernatant, "S2" (soluble cytoplasmic fraction), was set aside. The pellet, "P2," was resuspended in 5 mL of Buffer 2 (6 mM Tris [pH 8.1], 0.32 M sucrose, 1 mM EDTA, 1 mM EGTA, 1 mM DTT, supplemented with protease inhibitors). A sucrose gradient was prepared with the following layers, from bottom to top (10 mL of each): 1.2 M, 1.0 M, 0.85 M sucrose, each in 6 mM Tris [pH 8.1]. The P2 fraction was layered over the sucrose gradient and centrifuged for two hours at 82,500 g. Material at the interface between the 1.0 and 1.2 M layers was collected, diluted into 15 mL Buffer 2, and pelleted for 1 hr at 24,500 g. The pellet was resuspended in 0.5 mL of RIPA buffer containing 1 mM PMSF and protease inhibitor cocktail to give the "Synaptosome" fraction. Protein concentrations were analyzed by BCA assay and loaded equally (2 μg of protein) in each lane in Figure 5E.

For western blot analysis (Figure 5E), samples were loaded onto 8 or 12% SDS-PAGE (depending on the molecular weights of the protein of interest), transferred to nitrocellulose, and the membrane was blocked with 3% BSA TBST for 1 hr at room temperature. Antibodies were used as follows: rabbit anti-Tom20 (Santa Cruz 1:500), rabbit anti-NeuN (Abcam 1:1000), mouse anti-GluA1 (NeuromAb 1:1000), rabbit anti-Brinp3 (Santa Cruz 1:250), rabbit anti-Sema4a (Abcam 1:500), rabbit anti-Notch2 (Abcam 1:500), rabbit anti-5HT4 (Tpbg) (Abcam 1:500), rabbit anti-slc39a10 (Novus Biologicals 1:1000), rabbit anti-Itga6 (Abcam 1:500), rabbit anti-Egfr (Santa Cruz 1:500), mouse anti-synaptophysin (Sigma 1:2000), mouse anti-PSD95 (NeuromAb 1:1000), mouse anti-beta-actin (Sigma 1:2000). Secondary antibodies were: goat anti-mouse HRP conjugate (Bio-Rad, 1:3000 dilution) or goat anti-rabbit HRP conjugate (Bio-Rad, 1:3000 dilution). Blots were developed using Clarity Western ECL Substrate (Bio-Rad) and imaged on an Alpha Innotech gel documentation system.

Immunohistochemistry on Mouse Brain Tissue

For imaging endogenous Notch2 in Figure 5H, we blocked mouse tissue slices (a gift from G. Matthews and Kay Tye, MIT) in 5% (w/v) goat serum (Jackson Immunoresearch) in PBS overnight at 4°C with gentle rocking. Rabbit anti-Notch2 (Abcam, 1:500 dilution; same as antibody used for blotting of Notch2 in synaptosome fractions; recognizes a cytosolic region of Notch2) and mouse anti-Bassoon (Enzo Life sciences, 1:500 dilution) were diluted in 5% goat serum PBS, and incubated with the tissue sample overnight at 4°C. Then slices were washed three times with PBS at 4°C. Secondary antibodies goat anti-rabbit AlexaFluor-568 and goat anti-mouse AlexaFluor-647 (Invitrogen) were each diluted 1:000 in 5% goat serum PBS, and incubated with the slices overnight at 4°C. After three washes with PBS, the tissue was mounted onto Superfrost microscope slides (VWR) in Polyvinyl alcohol mounting medium with 1,4-Diazabicyclo[2.2.2]octane (Sigma) at 25°C overnight before imaging.

For CD200-related tissue imaging in Figures S6F–S6I, we prepared 14 μm sections, dried them, washed with PBS, then blocked with a 5% BSA + 0.2% Triton X-100 solution for 1-2 hr. Antibodies diluted in antibody buffer (150 mM NaCl, 50 mM Tris base, 5% BSA, 100 mM lysine and 0.04% sodium azide in 200 mL distilled water with pH adjusted to 7.4) were applied to sections for overnight incubation at 4°C. After three PBS washes, secondary antibodies diluted 1:250 in antibody buffer were added to slides and incubated for 2 hr at room temperature. Slides were then washed 3x in PBS and mounted with Vectashield + DAPI (Vector Labs) before imaging.

Antibody dilutions used were: CD200 (R+D systems, 1:250), Homer (Synaptic systems, 1:250), vGlut2 (Millipore, 1:1000).

MDGA Assays

Nlgn2 Synaptogenesis Assay, related to Figure 6B, 6C, and Figure S7B

Rat cortical neuron cultures were transfected at DIV12. To prepare DNA-Lipofectamine complexes, 1 μl of Lipofectamine 2000 per well (~150, 000 neurons), 50 ng of pCAG-V5-NLGN2A plasmid DNA, and 100 ng of one of the following: pCAG-Venus-MDGA1, pCAG-Venus-MDGA2, or pCAG-Venus were preincubated in 100 μl of MEM for 10 min. Most of the preconditioned growth media neurons were cultured in was removed and set aside, and the DNA-Lipofectamine complexes were added to the neurons. After 3 hr, all of the media was removed, and replaced with the previously set aside preconditioned growth media. Note that this assay is highly sensitive to plasmid stoichiometry, and we found that the MDGA plasmids must be provided in excess over NLGN2A plasmid. The media was then replaced with standard neuron culture media (Neurobasal containing B27, Glutamax, penicillin, streptomycin, and FUDR) and cells were cultured for 2 days before fixation and permeabilization for immunostaining with mouse anti-vGlut1 and rabbit anti-vGAT antibodies. For Figure S7B, neurons were processed similarly but transfected with 10 ng of pCAG-Venus plasmid, with either no additional DNA, or 100 ng of one of the following: pCAG-V5-NLGN2A, pCAG-V5-NLGN1, or pCAG-HRP-TM.

MDGA1/2 Knockdown Assay

For RNAi knockdown by plasmid-based short-hairpin RNA (shRNA), the oligonucleotides that target nucleotides 1027–1045 of rat MDGA1 (5′- GTCTCTTTCTTCTACCACA-3′) and 1933–1951 of rat MDGA2 (5′- AGGTGAAGCTAAAGAACAA-3′), were subcloned into LenLox3.7 variant pLLs-GFP to express GFP and shMDGA1/2 under the human synapsin promoter and U6 promoter, respectively. These hairpins had previously been used to knockdown MDGAs (Lee et al., 2013). We used shMORB (5′-GATGGTGGCAG TACCAGTG-3′) as a control shRNA (“scrambled”), which has no effects on neuronal morphology (Pettem et al., 2013). Lentiviruses were generated as described under “Lentivirus preparation and titration.”

Cortical rat neuron cultures at DIV7 were infected with shRNA-expressing lentiviruses. At DIV15, neurons were scraped and pelleted, and RNA was extracted using the RNeasy Mini Kit (QIAGEN) and analyzed by qPCR using the following primers for MDGA1; forward: 5′-ACCCCCGAAGGCTACTACAT-3′ and reverse: 5′-GGTTGAGGGAGCAGTAGAACT-3′, and the following primers for MDGA2; forward: 5′- CCCTCCAGAAGGTCCCACT-3′ and reverse: 5′-CGTCGGGGGAGCGTACA-3′ to assess extent of knockdown (Figure 6F). For the imaging assay in Figure 6E, after DIV7 infection of shRNA constructs, rescue constructs (RNAi-resistant mApple-MDGA1/2) were introduced by lentivirus at DIV11. At DIV15, the neurons were fixed, permeabilized, stained with anti-vGlut1 and anti-vGAT antibodies, and imaged by confocal microscopy, as described above (“Characterization of peroxidase fusion constructs by microscopy” and “Fluorescence microscopy”) with the exception of goat anti-mouse AlexaFluor405 replacing goat anti-mouse AlexaFluor488, and goat anti-rabbit AlexaFluor647 replacing goat anti-rabbit AlexaFluor568.

MDGA1/2 Overexpression Assay

Rat cortical neuron cultures were transfected at DIV12 using 1 μl of Lipofectamine 2000 per well (~150, 000 neurons) and 50 ng of one of the following: pCAG-Venus-MDGA1, pCAG-Venus-MDGA2, or Venus transfection marker exactly as described above under “Nlgn2 synaptogenesis assay.” Four days later, at DIV16, the neurons were fixed and stained for vGlut1 and vGAT markers as described above (“Characterization of peroxidase fusion constructs by microscopy”).

QUANTIFICATION AND STATISTICAL ANALYSIS

Quantification of Fluorescence Imaging Data

All fluorescence imaging data were acquired in confocal mode as described above (“Fluorescence microscopy”) except for the CD200 images so noted. The parameters quantified in this study were colocalization (with synaptic markers Bassoon, vGlut1, and vGAT), synapse density, and synapse size. To quantify colocalization, we used SlideBook 5.0 software to generate masks for each channel of interest (for example, the “BxxP” channel and the “vGlut1” channel). To generate masks consistently and without bias, we first calculated the mean intensity for each field of view (FOV) in a dataset, typically 8-15 images. From these mean intensities, we calculated the SD. We then set the mask threshold for each FOV at the mean intensity for that FOV plus 2x the SD. Once masked, we created an “intersection mask” from the individual channel masks.

To quantify colocalization of BxxP with synapse markers vGlut1 and vGAT (Figures 1D, 6A, S1D, S6D, S6E, S7A, and S7E), we counted the number of ROIs (regions of interest) in the intersection mask of “vGlut1” and “BxxP,” and in the intersection mask of “vGAT” and “BxxP.”

The % colocalization with vGlut1 was calculated as the number of ROIs in the vGlut1-BxxP intersection mask divided by the sum of ROIs in both vGlut1-BxxP and vGAT-BxxP intersection masks. Note that this analysis discards BxxP puncta that overlap with neither vGlut1 nor vGAT; such puncta may be at vGlut2 or vGlut3-sites, for example, that are not stained with our anti-vGlut1 antibody. % Colocalization with vGAT was calculated similarly.

To quantify % colocalization of BxxP with the general synapse marker Bassoon (Figures 5C and S2B) we calculated the total sum intensity of BxxP in the BxxP-Bassoon intersection mask, and divided by the total sum intensity of BxxP in the BxxP mask. This was repeated individually for each FOV in a dataset. From these % colocalization values, we calculated a mean colocalization and error, either SEM) or SD, as indicated in each figure legend.

To quantify synapse density, we created masks for vGlut1, vGAT, and Venus channels using the protocol described above. We created intersection masks between vGlut1 and Venus, and between vGAT and Venus. Within each of these intersection masks, we calculated the mean vGlut1 intensity and the mean vGAT intensity. These mean intensity values, reflecting vGlut1 or vGAT density over the transfected neurons, were averaged across all FOVs and the error was calculated as SEM. The data presented are normalized to the synapse density of the control sample.

The synapse size (Figure S3E) was calculated as the area of each ROI found in the vGlut1-GFP intersection mask or vGAT-GFP intersection mask. > 500 ROIs were analyzed per condition, and the area values were averaged and normalized to that of the control sample.

To quantify synapse numbers in the CD200 experiment (Figure S6I), we used a modified version of the protocol outlined in Hong et al., 2016. 14 μm sections stained with appropriate synaptic markers were imaged with a Zeiss LSM 700 confocal microscope as described above. Three fields of view were captured in both the ipsilateral and contralateral territories of the dLGN, and for each field a 3 μm z stack was imaged. ImageJ software was used to quantify the number of colocalized pre- and postsynaptic puncta in each z plane. Analysis was performed blind to genotype.

Statistics were performed using Graph Pad Prism. To compare datasets, we used an unpaired two-tailed Student’s T-Test. We considered differences significant when $p < 0.05$.

The exact value of “n” can be found within the figure legends describing each experiment.

Quantification of qPCR Data

We used qPCR to assess MDGA knockdown efficiencies (Figure 6F), and to measure increases in the levels of specific mRNAs upon heterologous introduction of HRP fusion proteins (Figure S3C). qPCR reactions were performed in triplicate on each biological sample. ΔC_t values (between target and GAPDH reference mRNA) were averaged, normalized to the control sample, and errors were calculated as SEM.

Replication

Apart from the large-scale proteomic experiment, which has been described in detail, each experiment in this study was fully replicated at least twice, from start to finish. These biological replicates were performed on different days, with different cells, and different aliquots of reagents. However, each figure in our study was generated from the data of only a single biological replicate.

Each biological replicate contained multiple (typically, 2 or more) technical replicates. For example, for an imaging experiment, each condition might be repeated across 2 or more wells across 2 or more cell culture dishes. For each condition, we would collect 8 or more fields of view from 2 or more distinct wells. We do not call these biological replicates, because these were all performed on the same day, in parallel, on the same batch of neurons harvested from the same rat. But the technical replicates are performed on independent wells and dishes.

Blinding at any Stage of the Study

Imaging data were analyzed blind to prevent any bias.

Sample-Size Estimation and Statistical Method of Computation

Sample sizes were chosen in order to obtain a normal distribution of the data. A Student's t test was applied because the distribution of data appeared to be normally distributed and the variables were unpaired.

Inclusion and Exclusion Criteria of any Data

No data were excluded during analysis.

DATA AND SOFTWARE AVAILABILITY

Data Resources

Mass spectra from the proteomic experiments may be downloaded from MassIVE (http://massive.ucsd.edu) using the identifier MSV000079849. The data are directly accessible via ftp://massive.ucsd.edu/MSV000079849.

ADDITIONAL RESOURCES

For detailed protocols on performing peroxidase proteomic mapping, see (Hung et al., 2016). The main differences between the protocols described therein, and the proteomic mapping described here in this study are: (1) HRP replaces APEX2; (2) BxxP replaces BP; (3) no BxxP preincubation required; (4) 1% SDS boiling treatment of cell lysate to dissociate PSDs; and (5) iTRAQ replaces SILAC.

The following genetic constructs used in this work are available via Addgene: HRP-LRRTM1; HRP-LRRTM2; HRP-NLGN2; HRP-SLITRK3; HRP-TM; HRP-MDGA1; HRP-MDGA2; CAG-Venus-MDGA1; CAG-Venus-MDGA2; and CAG-V5-NLGN2A.

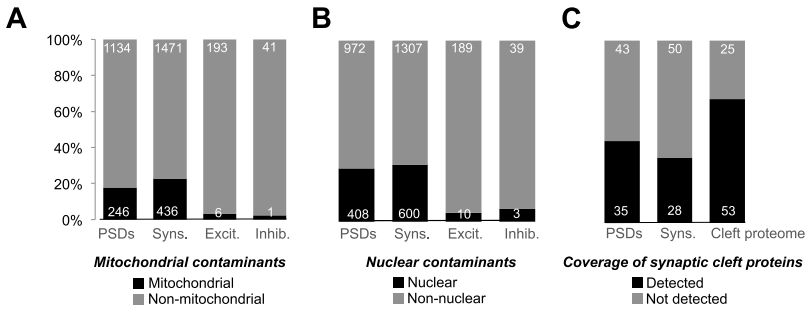

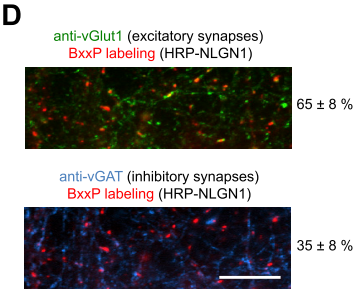

E

	Protein name	Gene name
1	Interleukin-1 receptor accessory protein-like 1	Il1rapl1
2	Glutamate receptor 2	Gria2
3	Isoform Flip of Glutamate receptor 2	Gria2
4	Glutamate receptor ionotropic, kainate 3	Grik3
5	Neuroligin-2	Nlgn2
6	Glutamate receptor ionotropic, NMDA 2B	Grin2b
7	Neuroligin-1	Nlgn1
8	Isoform B of Glutamate receptor ionotropic, NMDA 1	Grin1
9	Isoform 2 of Glutamate receptor 4	Gria4
10	Glutamate receptor ionotropic, NMDA 2A	Grin2a
11	Brain-specific angiogenesis inhibitor 3	Bai3
12	Protein Bai1	Bai1
13	Acid-sensing ion channel 1	Asic1
14	Neuropilin and tolloid-like protein 2	Neto2
15	Noelin-2	Olfm2
16	Voltage-dependent R-type calcium channel subunit alpha-1E	Cacna1e
17	Protein Cdh9	Cdh9
18	Gamma-aminobutyric acid receptor subunit beta-1	Gabrb1
19	Isoform 2 of Leucine-rich repeat-containing protein 7	Lrrc7
20	Gelsolin	Gsn
21	Protein Copa	Copa
22	Brain-specific angiogenesis inhibitor 2	Bai2
23	Isoform Flip of Glutamate receptor 1	Gria1
24	Gamma-aminobutyric acid receptor subunit alpha-5	Gabra5
25	Gamma-aminobutyric acid receptor subunit alpha-2	Gabra2
26	Inward rectifier potassium channel 4	Kcnj4
27	Protein disulfide-isomerase	P4hb
28	Down syndrome cell adhesion molecule homolog	Dscam
29	Leucine rich repeat containing 4C	Lrrc4c
30	Isoform Flip of Glutamate receptor 3	Gria3
31	Gamma-aminobutyric acid receptor subunit beta-3	Gabrb3
32	Protein Elfn1	ELFN1
33	Noelin	Olfm1
34	Protein Ptprd	Ptprd
35	Solute carrier family 12 member 5	Slc12a5
36	Protein Sez6l2	Sez6l2
37	Protein Igsf9b	Igsf9b
38	Metabotropic glutamate receptor 4	Grm4
39	Receptor-type tyrosine-protein phosphatase S	Ptprs
40	Leucine-rich repeat-containing protein 4	Lrrc4
41	Gamma-aminobutyric acid receptor subunit alpha-3	Gabra3
42	Pituitary adenylate cyclase-activating polypeptide type I receptor	Adcyap1r1
43	Gamma-aminobutyric acid receptor subunit beta-2	Gabrb2
44	Protein Fam171a2	Fam171a2
45	Netrin G2	Ntng2
46	Interleukin 1 receptor accessory protein b	Il1rap
47	Leucine-rich repeat-containing protein 4B	Lrrc4b
48	Glutamate receptor ionotropic, kainate 5	Grik5
49	Syntaxin-1B	Stx1b
50	Latrophilin-1	Lphn1

Figure S1. Comparison of Proteomes Derived from Biochemical Fractionation versus Peroxidase Tagging, and HRP-Nlgn1 Is Not Cleanly Localized to Excitatory Synapses, Related to Figures 1 and 4

(A) Fraction of each proteome with potential mitochondrial contamination. PSDs refers to the PSD proteome obtained by Bayés et al., 2012. Syns. refers to the synaptosome study by Biesemann et al., 2014. Excit. and Inhib. are our excitatory and inhibitory synaptic cleft proteomes. Mitochondrial versus non-mitochondrial is defined by annotation in GOCC. Note that the 7 proteins with mitochondrial annotation in our proteomes also have cell surface and synapse annotation (Nptx1, Prnp, Epha4, Brinp3, Bsg; and Erbb4 in both lists).

(B) Fraction of each proteome with potential nuclear contamination. Here, nuclear is defined by annotation in GOCC, but proteins that also have synapse annotation in GOCC are omitted. All 13 such proteins enriched in our datasets are known surface-localized proteins but may have a nuclear component as well, such as Notch2.

(C) Coverage of each proteome. Fraction of a true positive list of 78 established synaptic cleft proteins detected in each dataset. Cleft proteome refers to the combination of our Excit. and Inhib. lists. See also Table S3, Tabs 1-2 for details.

(D) Fluorescence microscopy of HRP-NLGN1 as in Figure 1D with vGlut1 and vGAT markers shows that this construct localizes to both excitatory and inhibitory synapses. Quantitation shown to the right of each image, calculated from 8 fields of view (containing > 900 puncta) per condition. Errors, ± 1 s.d. Scale bar, 10 um.

(E) Preliminary proteomic mapping experiment with HRP-NLGN1. Construct was introduced by lentivirus into DIV15 cortical neurons and subsequently labeled with BxxP at DIV19. The top 50 most enriched (by 114/116 iTRAQ ratio) cell-surface proteins (intracellular proteins have been removed, as this proteomic experiment was performed prior to development of the PSD-solubilizing protocol shown in Figure 2D) contain a ~2:1 mixture of excitatory synapse-annotated proteins (green) and inhibitory synapse-annotated proteins (red), which reflects HRP-NLGN1's excitatory/inhibitory localization ratio shown in (D).

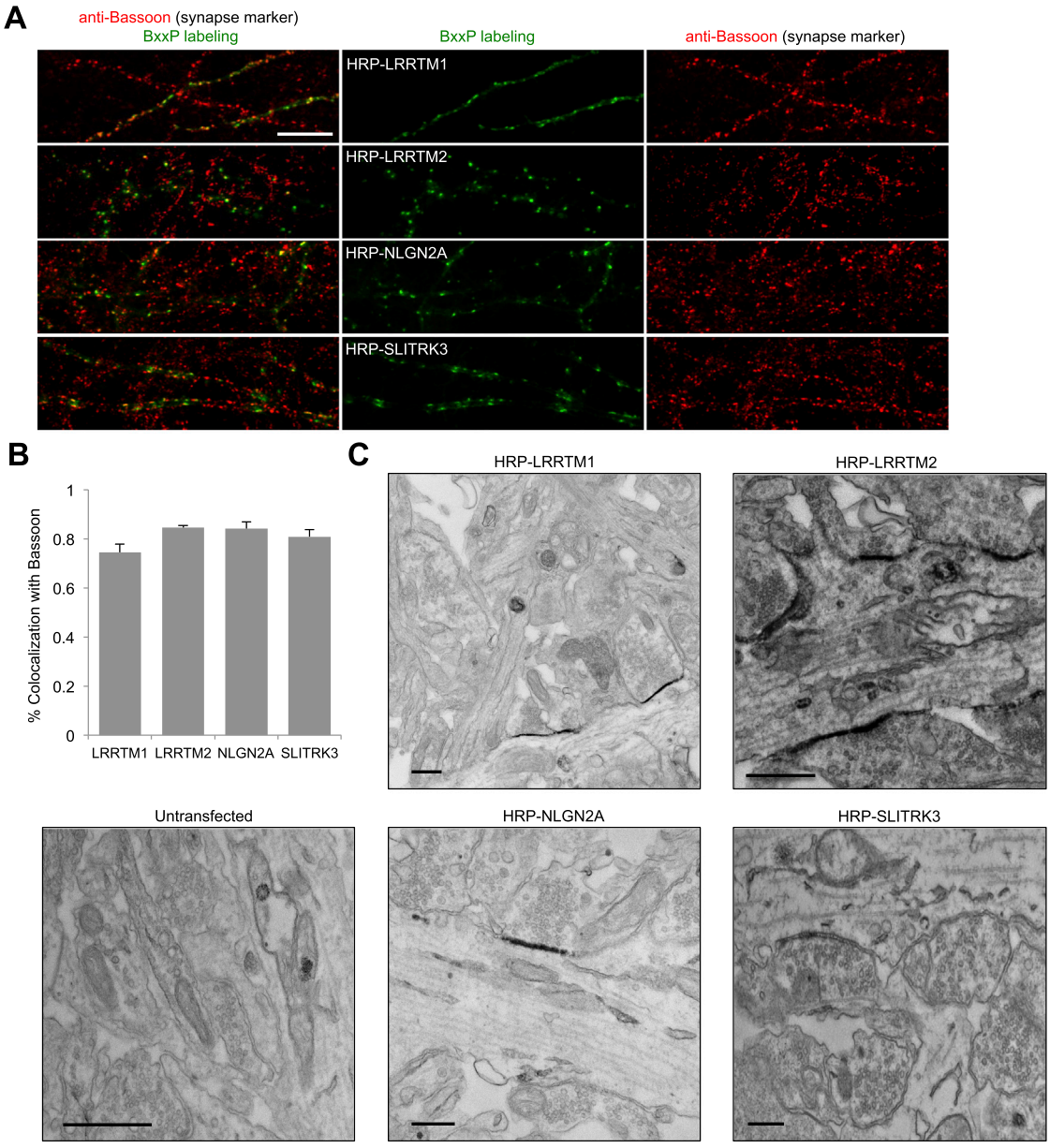

Figure S2. Further Characterization of HRP Fusion Constructs Used for Proteomic Tagging, Related to Figure 1

(A) Fluorescence imaging of HRP fusions with respect to Bassoon, an endogenous pre-synaptic marker. Dissociated rat cortical neurons at DIV19 expressing the indicated HRP fusion construct (introduced by lentiviral transduction as in Figure 1D) were labeled live with BxxP for 1 min, fixed, and stained with neutravidin-AlexaFluor647 (green) and anti-Bassoon antibody (AlexaFluor488 readout, red). Scale bars, 10 μm.

(B) Quantitation of data in (A) along with > 10 additional fields of view per sample. Errors, ± 1 SEM.

(C) Electron microscopy of HRP fusion constructs. Same as Figure 1F but zoomed out to show multiple synapses per field of view. Dark stain indicating the presence of HRP is restricted to cleft regions and not observed on dendritic or axonal surfaces outside of synapses. Images shown are representative of > 6 images per construct. Scale bars, 400 nm.

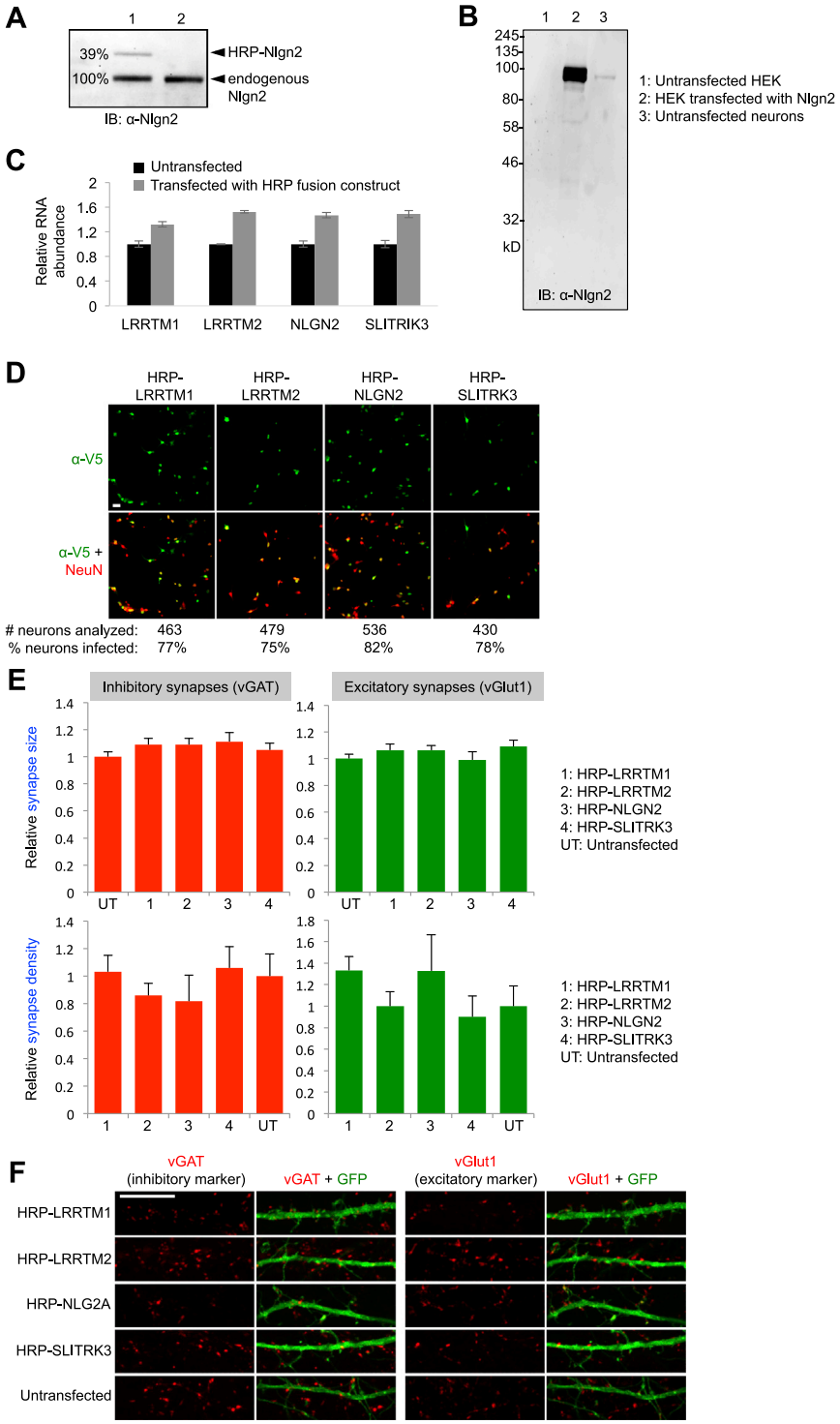

Figure S3. Expression Levels of Hrp Fusion Constructs Used for Proteomic Tagging, Related to Figure 1

(A) Western blot analysis of HRP-Nlgn2 protein expression. HRP-Nlgn2 was introduced by lentiviral transduction to DIV19 dissociated rat cortical neurons as in the MS proteomic experiment. Neuron lysates were run on SDS-PAGE and blotted with anti-Nlgn2 antibody. Lane 1 is the experiment, and lane 2 shows an uninfected negative control sample. Densitometry indicates that HRP-Nlgn2 was present at 39% of the level of endogenous Nlgn2. Accounting for the transduction efficiency of 82% (D), this corresponds to 1.5-fold overexpression in each transduced neuron.

(B) Validation of anti-Nlgn2 antibody by detection of recombinant Nlgn2 in HEK.

(legend continued on next page)

(C) qPCR analysis of mRNA levels with and without lentiviral transduction of HRP fusion constructs as in (A). qPCR primers were designed to amplify both the recombinant and endogenous genes. After correction for transduction efficiencies (D), the HRP constructs increase total mRNA levels by 1.4-1.7-fold in each neuron. Three technical replicates per construct; errors, ± 1 SEM.

(D) Determination of transduction efficiencies by anti-V5 staining of HRP fusion constructs and anti-NeuN staining of all neuron nuclei. Neurons were prepared and infected as in (A) and (C). Scale bar, 50 μm.

(E) Calculation of relative synapse size (top) and relative synapse density (bottom) in neurons with and without lentiviral introduction of HRP fusion constructs. Samples were prepared as in (A) and (C) with the following modifications: 1.3-fold more lentivirus was used in each case to achieve 97%–99% infection efficiency (data not shown). At DIV17, a GFP marker was introduced to a sparse subset of neurons (< 5%) by lipofectamine transfection. After fixation, neurons were stained for endogenous vGlut1 and vGAT as in Figure 1D. Synapse size was calculated as the area of vGlut1 or vGAT puncta overlapping with the GFP marker. > 500 puncta were analyzed per sample. Synapse density was calculated by first creating a mask based on GFP. We divided the total vGlut1 or vGAT intensity in that mask by the area of the mask; this was repeated for > 13 fields of view per sample. Errors, ± 1 SEM.

(F) Representative images of neurons quantified in (E). Scale bar, 10 μm.

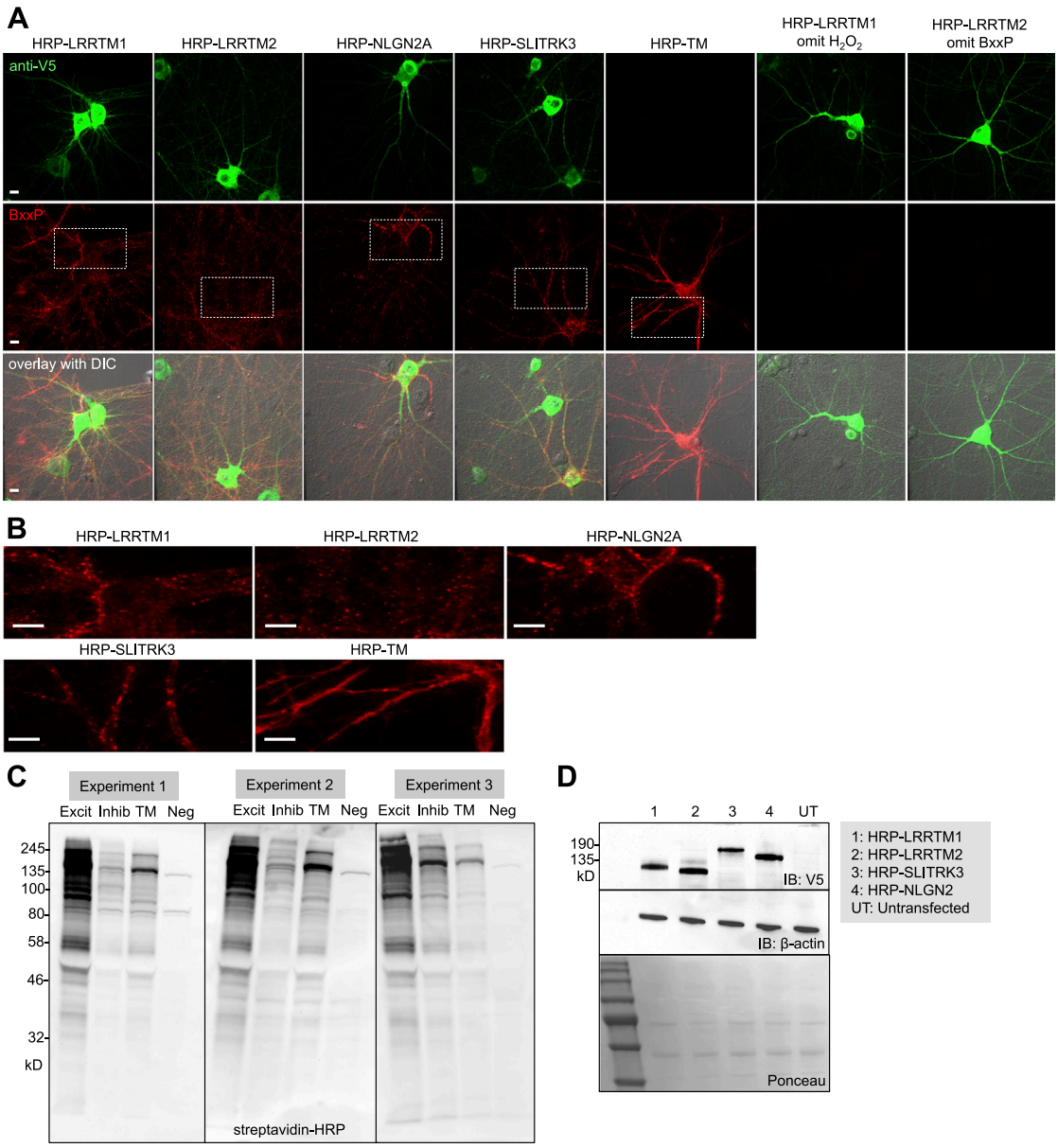

Figure S4. Characterizing the Biotinylation Activities of Synaptic HRP Fusion Constructs, Related to Figures 1 and 2

(A) Fluorescence imaging of the biotinylation catalyzed by HRP fusion constructs used for proteomics. DIV19 rat cortical neurons expressing the constructs indicated across the top were treated with BxxP and H_2O_2 for 1 min, then fixed and stained with neutravidin-AlexaFluor647 to detect biotinylated proteins (middle row) and anti-V5 antibody (AlexaFluor 488 readout) to detect HRP construct expression (top row). Note that our staining conditions highlight the *surface* pool of biotinylated proteins, but the *total* pool of V5-tagged HRP constructs. The last two columns show negative controls with H_2O_2 or BxxP omitted. DIC, differential interference contrast.

(B) Zoomed-in views of boxed regions in (A). Synaptic constructs show punctate BxxP labeling, whereas HRP-TM gives a diffuse staining pattern. Scale bars, 10 um.

(C) Streptavidin blot analysis of whole neuron lysates infected and labeled with BxxP as in Figure 2B. The three bands in the negative control lanes at 129, 81, and 79 kDa are endogenously biotinylated proteins (Chapman-Smith and Cronan, 1999).

(D) Relative expression levels of the HRP fusion constructs. Samples were prepared as in (C), then stained with anti-V5 antibody to visualize the HRP fusion constructs. Endogenous actin is stained in the same lysates for reference.

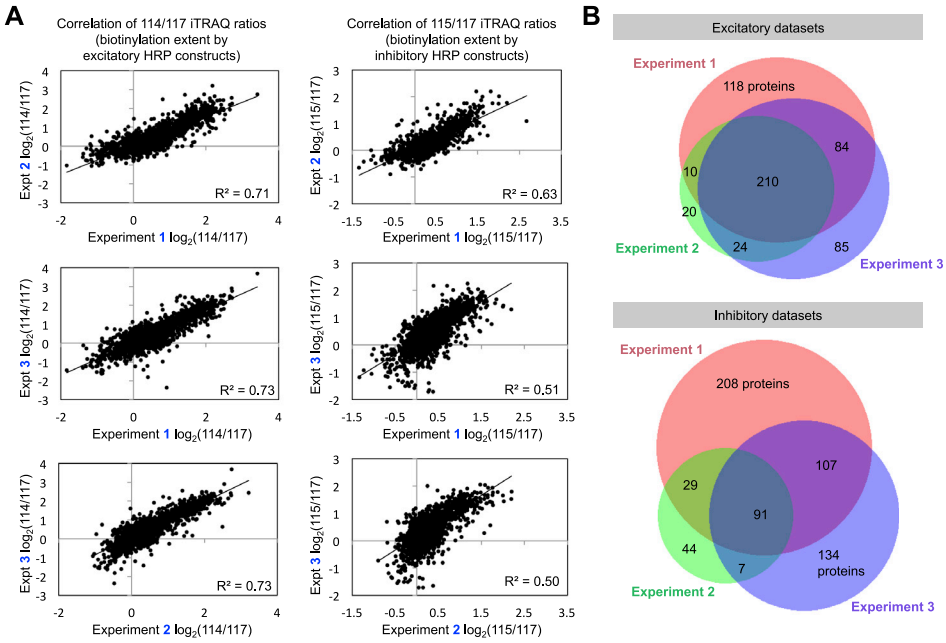

C

Dataset	# of proteins	Specificity	Coverage
Experiment 1 (E1)	422	57.3%	80.6%
Experiment 2 (E2)	264	69.6%	77.4%
Experiment 3 (E3)	403	62.3%	80.6%
E1 ∩ E2	220	73.2%	70.9%
E1 ∩ E3	294	65.0%	75.8%
E2 ∩ E3	234	72.6%	70.9%
E1 ∩ E2 ∩ E3	210	73.8%	69.3%
Union of E1 & E2 & E3	551	58.0%	85.5%

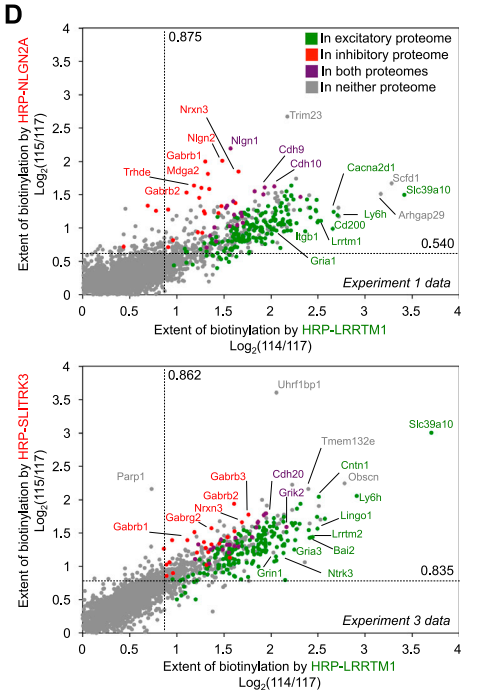

Figure S5. Further Analysis of the Proteomic Data, Related to Figure 3

(A) Scatterplots showing correlation of iTRAQ ratios across independent experiments.

(B) Venn diagrams showing overlap between datasets, after application of Filters 1 and 2, but before application of Filter 3.

(C) Table showing increase in specificity and decrease in coverage as data from independent experiments are intersected to produce excitatory synaptic cleft proteomes. As in (B), Filters 1 and 2 have been applied to these datasets, but not Filter 3. Here, specificity is defined as the fraction of proteins with synapse annotation in GOCC, Synaptome DB, the Biesemann et al., 2014 synaptosome MS study, the Bayés et al., 2012 PSD MS study, or the Boyken et al., 2013 active zone MS study. The specificity calculation here does not include additional proteins with literature connection to synapses discovered by manual searching, as we performed for our final proteomic list. Coverage is based on a true positive list of 62 well-established excitatory synaptic cleft proteins (Table S3, Tab 1).

(D) Same as scatterplot in Figure 4D, except for Experiment 1 and 3 datasets, instead of Experiment 2.

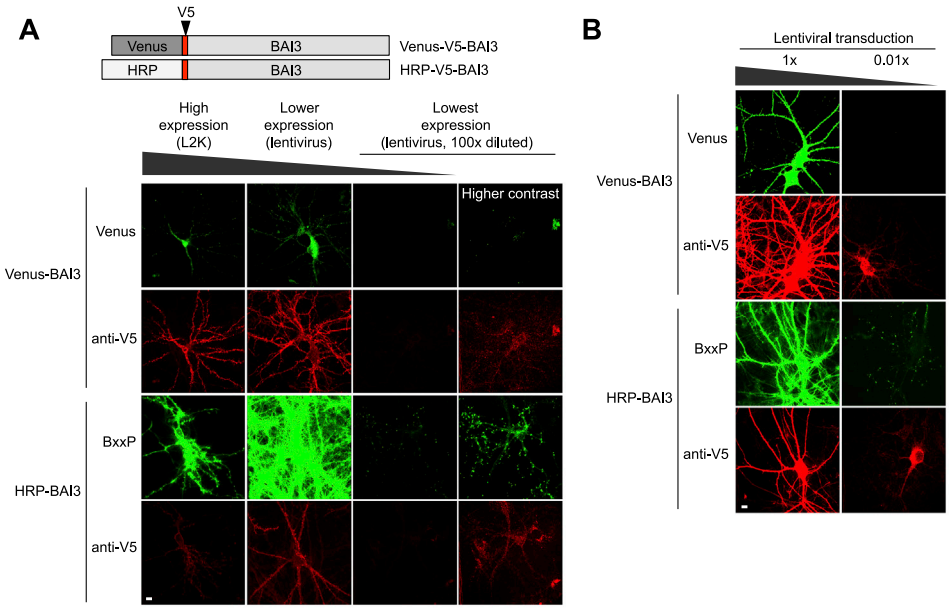

C

Synapse subtype orphans	Literature annotation	Literature reference	Our proteomic data	Our imaging data
Leucine-rich repeat transmembrane protein FLRT2	E	O'Sullivan et al. 2012	E & I	E & I (Fig. S7D)
Ephrin type-B receptor 6 (EPHB6)	E	Biesemann et al. 2014	E & I	E & I (Fig. S7D)
Netrin receptor DCC	E	Goldman et al. 2013	E & I	E & I (Fig. S7D)
ELFN1	E	Sylwestrak & Ghosh 2012	E & I	E & I (Fig. S7E)
Neuroligin-1 (NLGN1)	E	Song et al. 1999	E & I	E & I (Fig. S2A)
MDGA1	I	Pattem et al. 2013; Lee et al. 2013	E	E & I (Fig. S8A)

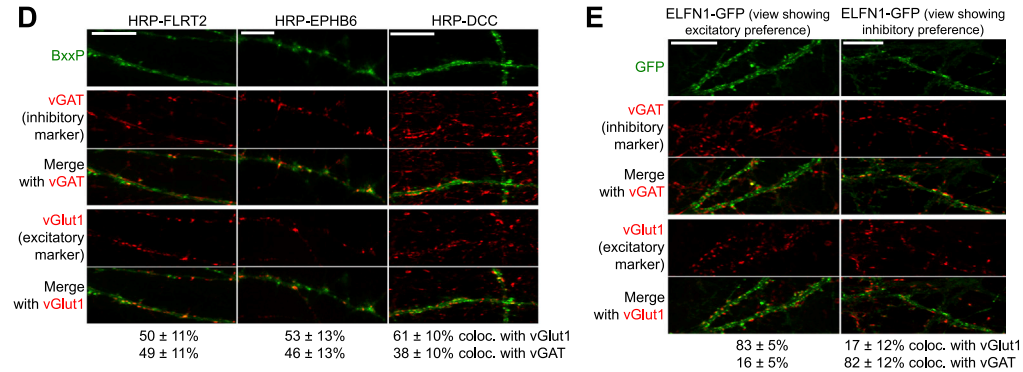

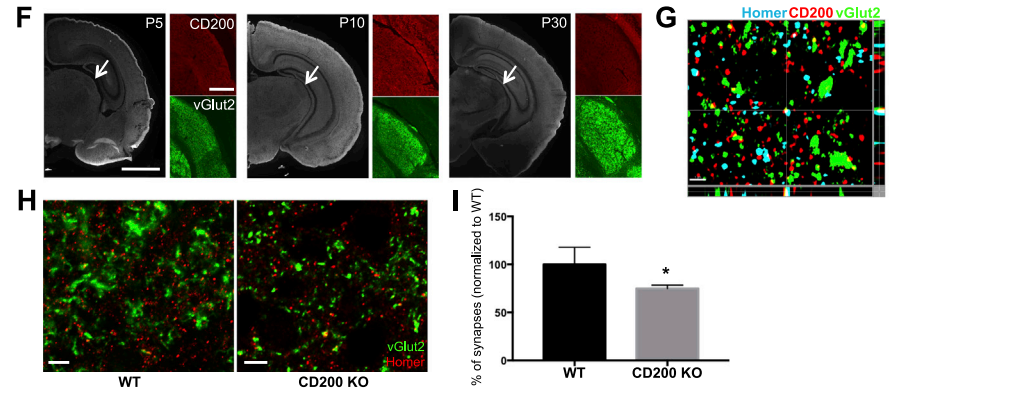

(legend on next page)

Figure S6. Fluorescence Imaging of Synapse Sub-Type Orphans and Analysis Of CD200 at Excitatory Synapses, Related to Figure 5

(A) The HRP tag is superior to Venus fluorescent protein for detection of surface proteins at low expression levels. The tagged BAI3 fusion constructs shown at top were introduced to cultured neurons in three expression level regimes: highest, via lipofectamine transfection; lower, via lentiviral transduction; and lowest, via lentiviral transduction but with 100-fold less virus. The last column is the same as the third column, but the intensity scale is narrowed to show the images at higher contrast. At DIV19, neurons were labeled live with BxxP, then fixed without permeabilization and stained with neutravidin-AlexaFluor647 to detect biotinylated proteins and anti-V5 antibody (AlexaFluor568 readout) to detect the V5 tag. Whereas HRP-BAI3 puncta are visible, Venus-BAI3 puncta cannot be detected in the lowest expression regime. Scale bar, 10 μm.

(B) Same as A, except the anti-V5 staining was performed after cell permeabilization, in order to detect total protein pools rather than cell surface pools only. Scale bar, 10 μm.

(C) Table summarizing data on synapse sub-type orphans, which are proteins known to be generally synaptic, but their synapse sub-type localization preferences are unknown or incomplete. E, excitatory. I, inhibitory.

(D) Imaging of synapse subtype orphans Flrt2, Ephb6, and Dcc. Orphan genes were fused at their N-terminal ends to HRP, and expressed via lentiviral transduction in DIV19 dissociated rat cortical neurons. The HRP tag was visualized by live BxxP labeling, followed by neutravidin-AlexaFluor647 staining on fixed cells. Endogenous vGAT and vGlut1 were detected with respective antibodies followed by AlexaFluor488 and AlexaFluor568 readout.

(E) Imaging of Elfn1-GFP in DIV19 rat cortical neuron cultures (lentiviral transduction). vGAT and vGlut1 were detected as in (D). Within the same culture dish, Elfn1 appeared at excitatory synapses in some fields of view (left), and at inhibitory synapses in other fields of view (right). > 13 fields of view were analyzed per construct shown in (D) and (E); scale bars 10 μm; errors, ± 1 s.d.

(F) Representative images of CD200 immunostaining in coronal sections of wild-type mouse brain. CD200 is localized throughout the neuropil and is most highly expressed during periods of synapse development and remodeling (left). Arrow denotes the dorsolateral geniculate nucleus (dLGN). Scale bar, 1 mm. Magnified images of the dLGN demonstrate that CD200 levels peak at P10 in this region (right, red (AlexaFluor594)). Presynaptic marker vGlut2 labels retinogeniculate synapses and can be used to visualize the dLGN (right, green (AlexaFluor488)). Scale bar, 200 μm.

(G) Representative structured illumination microscopy (SIM) image of CD200 (red; AlexaFluor594) in the P10 dLGN showing colocalization with presynaptic vGlut2 (green; AlexaFluor488) and postsynaptic Homer (cyan; AlexaFluor647). Orthogonal views confirm CD200 colocalization with an excitatory synapse (right and bottom edges). Scale bar, 1 μm.

(H) Representative confocal images of pre- and postsynaptic markers of retinogeniculate synapses in the dLGN of P10 CD200 knock out (KO) mice and wild-type (WT) littermates. Scale bar, 5 μm. Note the reduced number of colocalized puncta (denoting synapses; AlexaFluor488 and AlexaFluor594) in the CD200 KO.

(I) Quantification of retinogeniculate synapse numbers in CD200 KO mice relative to synapse numbers in WT littermate controls. There are significantly fewer retinogeniculate synapses in the dLGN of P10 CD200 KO mice *$p < 0.05$ ($n = 4$ WT and 5 CD200 KO). Error bars, SEM.

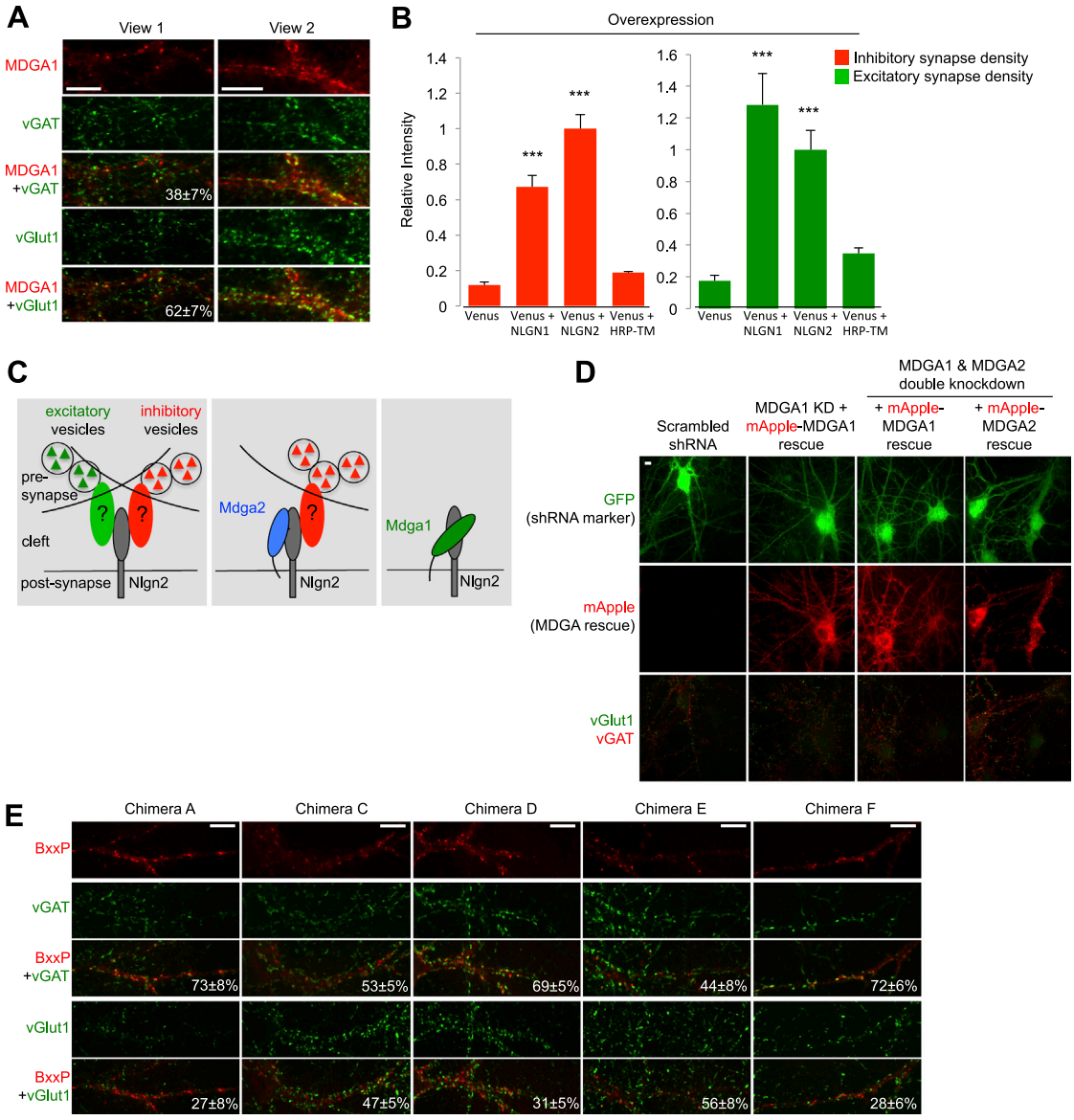

Figure S7. Additional Data Related to Mdga1 and Mdga2, Related to Figure 6

(A) Localization of HRP-MDGA1 to both excitatory and inhibitory synapses. Samples were prepared and imaged as in Figure 6A. Colocalization was quantified from 8 fields of view; errors, ± 1 s.d; scale bar, 10 μm.

(B) Validation of NLGN2 synaptogenesis assay used in Figure 6B. Overexpression of either NLGN1 or NLGN2 leads to enhanced recruitment of both excitatory and inhibitory synaptic vesicles. Samples were prepared, imaged, and quantified as in Figure 6C. HRP-TM is used as a non-synaptogenic negative control. 8 fields of view were analyzed per condition. Errors, ± SEM; *** indicates $p < 0.0001$ (Student's t test).

(C) Possible model for Mdga1 versus Mdga2 action via Nlgn2 at synapses. Through unknown presynaptic binding partners, Nlgn2 can recruit both inhibitory and excitatory presynaptic terminals (left panel). Mdga2 may bind to Nlgn2 in *cis* to selectively downregulate its recruitment of excitatory vesicles but not inhibitory vesicles (middle). In contrast, Mdga1 may bind to Nlgn2 in *cis* to downregulate its recruitment of both vesicle types (right panel). This activity may serve to both regulate inhibitory synapse size and prevent invasion of Nlgn2 into excitatory synapses.

(D) Fluorescence images associated with knockdown and rescue experiment shown in Figure 6E. shRNAs and GFP marker were introduced by lentiviral transduction at DIV7, and rescue constructs (mApple-MDGA1 or mApple-MDGA2) were introduced by lentivirus at DIV11. At DIV15, neurons were fixed and stained with anti-vGlut1 and anti-vGAT antibodies. Scale bar, 10 μm.

(E) Imaging of Mdga1/Mdga2 chimeras. Related to Figures 6G-H. N-terminal HRP-tagged chimeras were imaged and quantified as in (A). Colocalization values are based on these images and an additional 5 fields of view not shown (with > 300 puncta) per construct. Errors, ± 1 s.d. Scale bars, 10 μm.